

The mutational constraint spectrum quantified from variation in 141,456 humans


<https://doi.org/10.1038/s41586-020-2308-7>

Received: 27 January 2019

Accepted: 26 March 2020

Published online: 27 May 2020

Open access

 Check for updates

Konrad J. Karczewski^{1,2,✉}, Laurent C. Francioli^{1,2}, Grace Tiao^{1,2}, Beryl B. Cummings^{1,2,3}, Jessica Alfoldi^{1,2}, Qingbo Wang^{1,2,4}, Ryan L. Collins^{1,4,5}, Kristen M. Laricchia^{1,2}, Andrea Ganna^{1,2,6}, Daniel P. Birnbaum^{1,2}, Laura D. Gauthier⁷, Harrison Brand^{1,5}, Matthew Solomonson^{1,2}, Nicholas A. Watts^{1,2}, Daniel Rhodes⁸, Moriel Singer-Berk^{1,2}, Eleina M. England^{1,2}, Eleanor G. Seaby^{1,2}, Jack A. Kosmicki^{1,2,4}, Raymond K. Walters^{1,2,9}, Katherine Tashman^{1,2,9}, Yossi Farjoun⁷, Eric Banks⁷, Timothy Poterba⁷, Arcturus Wang^{1,2,9}, Cotton Seed^{1,2,9}, Nicola Whiffin^{1,2,10,11}, Jessica X. Chong¹², Kaitlin E. Samocha¹³, Emma Pierce-Hoffman^{1,2}, Zachary Zappala^{1,2,14}, Anne H. O'Donnell-Luria^{1,2,15,16}, Eric Vallabh Minikel¹, Ben Weisburd⁷, Monkol Lek¹⁷, James S. Ware^{1,10,11}, Christopher Vittal^{2,9}, Irina M. Armean^{1,2}, Louis Bergelson⁷, Kristian Cibulskis⁷, Kristen M. Connolly¹⁸, Miguel Covarrubias⁷, Stacey Donnelly¹, Steven Ferriera¹⁸, Stacey Gabriel¹⁸, Jeff Gentry⁷, Namrata Gupta^{1,18}, Thibault Jeandet⁷, Diane Kaplan⁷, Christopher Llanwarne⁷, Ruchi Munshi⁷, Sam Novod⁷, Nikelle Petrillo⁷, David Roazen⁷, Valentin Ruano-Rubio⁷, Andrea Saltzman¹, Molly Schleicher¹, Jose Soto⁷, Kathleen Tibbetts⁷, Charlotte Tolonen⁷, Gordon Wade⁷, Michael E. Talkowski^{1,5,19}, Genome Aggregation Database Consortium*, Benjamin M. Neale^{1,2,9}, Mark J. Daly^{1,2,6,9} & Daniel G. MacArthur^{1,2,14,9,15,16,✉}

Genetic variants that inactivate protein-coding genes are a powerful source of information about the phenotypic consequences of gene disruption: genes that are crucial for the function of an organism will be depleted of such variants in natural populations, whereas non-essential genes will tolerate their accumulation. However, predicted loss-of-function variants are enriched for annotation errors, and tend to be found at extremely low frequencies, so their analysis requires careful variant annotation and very large sample sizes¹. Here we describe the aggregation of 125,748 exomes and 15,708 genomes from human sequencing studies into the Genome Aggregation Database (gnomAD). We identify 443,769 high-confidence predicted loss-of-function variants in this cohort after filtering for artefacts caused by sequencing and annotation errors. Using an improved model of human mutation rates, we classify human protein-coding genes along a spectrum that represents tolerance to inactivation, validate this classification using data from model organisms and engineered human cells, and show that it can be used to improve the power of gene discovery for both common and rare diseases.

The physiological function of most genes in the human genome remains unknown. In biology, as in many engineering and scientific fields, breaking the individual components of a complex system can provide valuable insight into the structure and behaviour of that system. For the discovery of gene function, a common approach is to introduce disruptive mutations into genes and determine their effects on cellular and physiological phenotypes in mutant organisms or cell lines². Such studies have yielded valuable insight into eukaryotic physiology and

have guided the design of therapeutic agents³. However, although studies in model organisms and human cell lines have been crucial in deciphering the function of many human genes, they remain imperfect proxies for human physiology.

Obvious ethical and technical constraints prevent the large-scale engineering of loss-of-function mutations in humans. However, recent exome and genome sequencing projects have revealed a surprisingly high burden of natural pLoF variation in the human population,

¹Program in Medical and Population Genetics, Broad Institute of MIT and Harvard, Cambridge, MA, USA. ²Analytic and Translational Genetics Unit, Massachusetts General Hospital, Boston, MA, USA. ³Program in Biological and Biomedical Sciences, Harvard Medical School, Boston, MA, USA. ⁴Program in Bioinformatics and Integrative Genomics, Harvard Medical School, Boston, MA, USA. ⁵Center for Genomic Medicine, Massachusetts General Hospital, Boston, MA, USA. ⁶Institute for Molecular Medicine Finland, Helsinki, Finland. ⁷Data Sciences Platform, Broad Institute of MIT and Harvard, Cambridge, MA, USA. ⁸Centre for Translational Bioinformatics, William Harvey Research Institute, Barts and the London School of Medicine and Dentistry, Queen Mary University of London and Barts Health NHS Trust, London, UK. ⁹Stanley Center for Psychiatric Research, Broad Institute of MIT and Harvard, Cambridge, MA, USA. ¹⁰National Heart & Lung Institute and MRC London Institute of Medical Sciences, Imperial College London, London, UK. ¹¹Cardiovascular Research Centre, Royal Brompton & Harefield Hospitals NHS Trust, London, UK. ¹²Department of Pediatrics, University of Washington, Seattle, WA, USA. ¹³Wellcome Sanger Institute, Wellcome Genome Campus, Hinxton, Cambridge, UK. ¹⁴Vertex Pharmaceuticals Inc, Boston, MA, USA. ¹⁵Division of Genetics and Genomics, Boston Children's Hospital, Boston, MA, USA. ¹⁶Department of Pediatrics, Harvard Medical School, Boston, MA, USA. ¹⁷Department of Genetics, Yale School of Medicine, New Haven, CT, USA. ¹⁸Broad Genomics, Broad Institute of MIT and Harvard, Cambridge, MA, USA. ¹⁹Department of Neurology, Harvard Medical School, Boston, MA, USA. ²⁰Present address: Centre for Population Genomics, Garvan Institute of Medical Research, and UNSW Sydney, Sydney, New South Wales, Australia. ²¹Present address: Centre for Population Genomics, Murdoch Children's Research Institute, Melbourne, Victoria, Australia. *Lists of authors and their affiliations appear at the end of the paper. ✉e-mail: konradk@broadinstitute.org; d.macarthur@garvan.org.au

including stop-gained, essential splice, and frameshift variants^{1,4}, which can serve as natural models for inactivation of human genes. Such variants have already revealed much about human biology and disease mechanisms, through many decades of study of the genetic basis of severe Mendelian diseases⁵, most of which are driven by disruptive variants in either the heterozygous or homozygous state. These variants have also proved valuable in identifying potential therapeutic targets: confirmed LoF variants in the *PCSK9* gene have been causally linked to low levels of low-density lipoprotein cholesterol⁶, and have ultimately led to the development of several inhibitors of PCSK9 that are now in clinical use for the reduction of cardiovascular disease risk. A systematic catalogue of pLoF variants in humans and the classification of genes along a spectrum of tolerance to inactivation would provide a valuable resource for medical genetics, identifying candidate disease-causing mutations, potential therapeutic targets, and windows into the normal function of many currently uncharacterized human genes.

Several challenges arise when assessing LoF variants at scale. LoF variants are on average deleterious, and are thus typically maintained at very low frequencies in the human population. Systematic genome-wide discovery of these variants requires whole-exome or whole-genome sequencing of very large numbers of samples. In addition, LoF variants are enriched for false positives compared with synonymous or other benign variants, including mapping, genotyping (including somatic variation), and particularly, annotation errors¹, and careful filtering is required to remove such artefacts.

Population surveys of coding variation enable the evaluation of the strength of natural selection at a gene or region level. As natural selection purges deleterious variants from human populations, methods to detect selection have modelled the reduction in variation (constraint)⁷ or shift in the allele frequency distribution⁸, compared to an expectation. For analyses of selection on coding variation, synonymous variation provides a convenient baseline, controlling for other potential population genetic forces that may influence the amount of variation as well as technical features of the local sequence. A model of constraint was previously applied to define a set of 3,230 genes with a high probability of intolerance to heterozygous pLoF variation (pLI)⁴ and estimated the selection coefficient for variants in these genes⁹. However, the ability to comprehensively characterize the degree of selection against pLoF variants is particularly limited, as for small genes, the expected number of mutations is still very low, even for samples of up to 60,000 individuals^{4,10}. Furthermore, the previous dichotomization of pLI, although convenient for the characterization of a set of genes, disguises variability in the degree of selective pressure against a given class of variation and overlooks more subtle levels of intolerance to pLoF variation. With larger sample sizes, a more accurate quantitative measure of selective pressure is possible.

Here, we describe the detection of pLoF variants in a cohort of 125,748 individuals with whole-exome sequence data and 15,708 individuals with whole-genome sequence data, as part of the Genome Aggregation Database (gnomAD; <https://gnomad.broadinstitute.org>), the successor to the Exome Aggregation Consortium (ExAC). We develop a continuous measure of intolerance to pLoF variation, which places each gene on a spectrum of LoF intolerance. We validate this metric by comparing its distribution to several orthogonal indicators of constraint, including the incidence of structural variation and the essentiality of genes as measured using mouse gene knockout experiments and cellular inactivation assays. Finally, we demonstrate that this metric improves the interpretation of genetic variants that influence rare disease and provides insight into common disease biology. These analyses provide, to our knowledge, the most comprehensive catalogue so far of the sensitivity of human genes to disruption.

In a series of accompanying manuscripts, other complementary analyses of this dataset are described. Using an overlapping set of 14,237 whole genomes, the discovery and characterization of a wide variety of structural variants (large deletions, duplications, insertions, or other

rearrangements of DNA) is reported¹¹. The value of pLoF variants for the discovery and validation of therapeutic drug targets is explored¹², and a case study of the use of these variants from gnomAD and other large reference datasets is provided to validate the safety of inhibition of LRRK2—a candidate therapeutic target for Parkinson's disease¹³. By combining the gnomAD dataset with a large collection of RNA sequencing data from adult human tissues¹⁴, the value of tissue expression data in the interpretation of genetic variation across a range of human diseases is reported¹⁵. Finally, the effect of two understudied classes of human variation—multi-nucleotide variants¹⁶ and variants that create or disrupt open-reading frames in the 5' untranslated region of human genes—is characterized and investigated¹⁷.

A high-quality catalogue of variation

We aggregated whole-exome sequencing data from 199,558 individuals and whole-genome sequencing data from 20,314 individuals. These data were obtained primarily from case-control studies of common adult-onset diseases, including cardiovascular disease, type 2 diabetes and psychiatric disorders. Each dataset, totalling more than 1.3 and 1.6 petabytes of raw sequencing data, respectively, was uniformly processed, joint variant calling was performed on each dataset using a standardized BWA-Picard-GATK pipeline¹⁸, and all data processing and analysis was performed using Hail¹⁹. We performed stringent sample quality control (Extended Data Fig. 1), removing samples with lower sequencing quality by a variety of metrics, samples from second-degree or closer related individuals across both data types, samples with inadequate consent for the release of aggregate data, and samples from individuals known to have a severe childhood-onset disease as well as their first-degree relatives. The final gnomAD release contains genetic variation from 125,748 exomes and 15,708 genomes from unique unrelated individuals with high-quality sequence data, spanning 6 global and 8 sub-continental ancestries (Fig. 1a, b), which we have made publicly available at <https://gnomad.broadinstitute.org>. We also provide subsets of the gnomAD datasets, which exclude individuals who are cases in case-control studies, or who are cases of a few particular disease types such as cancer and neurological disorders, or who are also aggregated in the **Bravo TOPMed variant browser** (<https://bravo.sph.umich.edu>).

Among these individuals, we discovered 17.2 million and 261.9 million variants in the exome and genome datasets, respectively; these variants were filtered using a custom random forest process (Supplementary Information) to 14.9 million and 229.9 million high-quality variants. Comparing our variant calls in two samples for which we had independent gold-standard variant calls, we found that our filtering achieves very high precision (more than 99% for single nucleotide variants (SNVs), over 98.5% for indels in both exomes and genomes) and recall (over 90% for SNVs and more than 82% for indels for both exomes and genomes) at the single sample level (Extended Data Fig. 2). In addition, we leveraged data from 4,568 and 212 trios included in our exome and genome call-sets, respectively, to assess the quality of our rare variants. We found that our model retains over 97.8% of the transmitted singletons (singletons in the unrelated individuals that are transmitted to an offspring) on chromosome 20 (which was not used for model training) (Extended Data Fig. 3a–d). In addition, the number of putative de novo calls after filtering are in line with expectations²⁰ (Extended Data Fig. 3e–h), and our model had a recall of 97.3% for de novo SNVs and 98% for de novo indels based on 375 independently validated de novo variants in our whole-exome trios (295 SNVs and 80 indels) (Extended Data Fig. 3i, j). Altogether, these results indicate that our filtering strategy produced a call-set with high precision and recall for both common and rare variants.

These variants reflect the expected patterns based on mutation and selection: we observe 84.9% of all possible consistently methylated CpG-to-TpG transitions that would create synonymous variants in the human exome (Supplementary Table 14), which indicates that at this

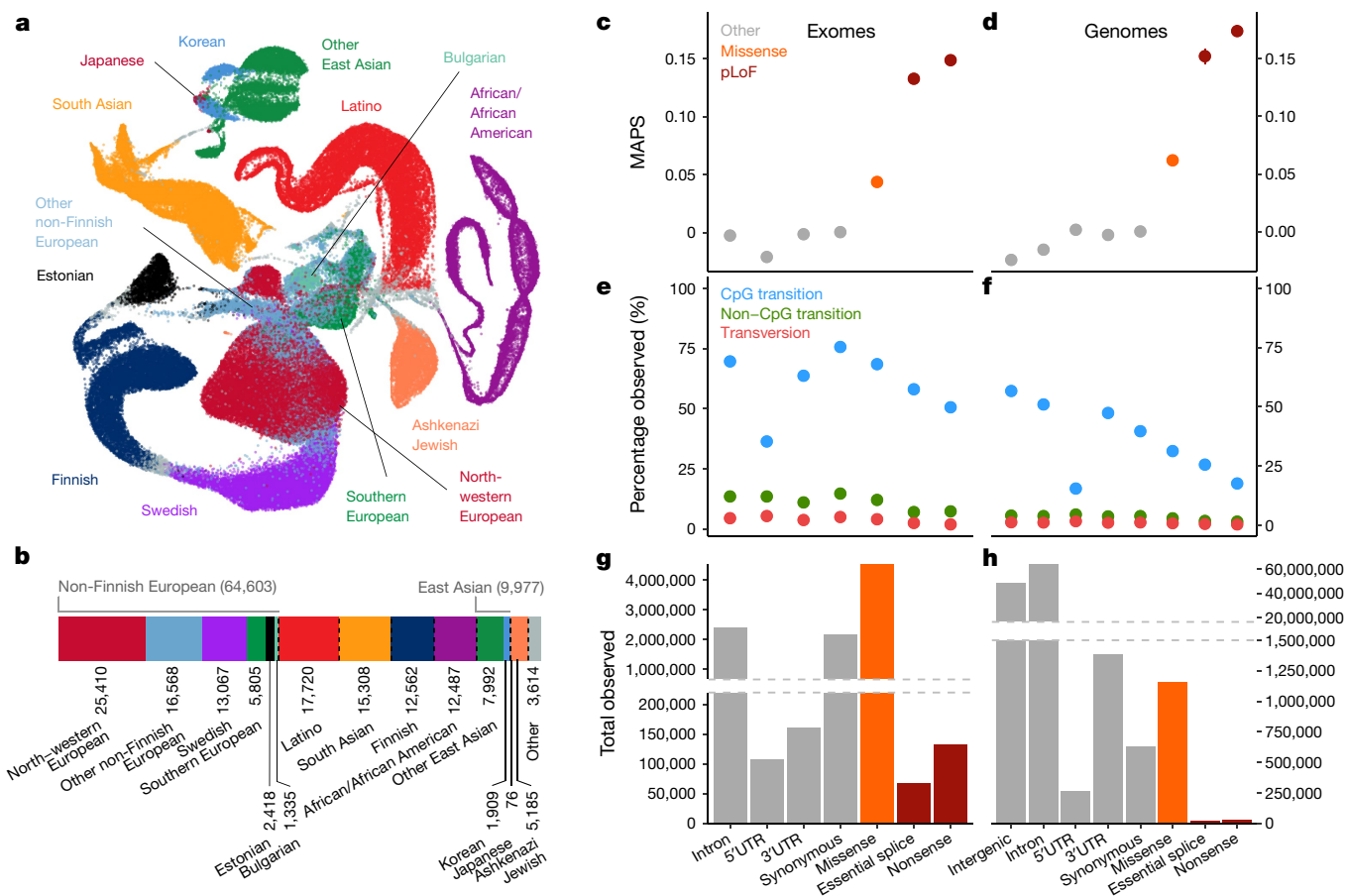


Fig. 1 | Aggregation of 141,456 exome and genome sequences. **a**, Uniform manifold approximation and projection (UMAP)^{46,47} plot depicting the ancestral diversity of all individuals in gnomAD, using ten principal components. Note that long-range distances in the UMAP space are not a proxy for genetic distance. **b**, The number of individuals by population and subpopulation in the gnomAD database. Colours representing populations in **a** and **b** are consistent. **c**, **d**, The mutability-adjusted proportion of singletons⁴ (MAPS) is shown across functional categories for SNVs in exomes (**c**; x axis shared with **e** and **g**) and genomes (**d**; x axis shared with **f** and **h**). Higher values

indicate an enrichment of lower frequency variants, which suggests increased deleteriousness. **e**, **f**, The proportion of possible variants observed for each functional class for exomes (**e**) and genomes (**f**). CpG transitions are more saturated, except where selection (for example, pLoFs) or hypomethylation (5' untranslated region) decreases the number of observations. **g**, **h**, The total number of variants observed in each functional class for exomes (**g**) and genomes (**h**). Error bars in **c**–**f** represent 95% confidence intervals (note that in some cases these are fully contained within the plotted point).

sample size, we are beginning to approach mutational saturation of this highly mutable and weakly negatively selected variant class. However, we only observe 52% of methylated CpG stop-gained variants, which illustrates the action of natural selection removing a substantial fraction of gene-disrupting variants from the population (Fig. 1c–h). Across all mutational contexts, only 11.5% and 3.7% of the possible synonymous and stop-gained variants, respectively, are observed in the exome dataset, which indicates that current sample sizes remain far from capturing complete mutational saturation of the human exome (Extended Data Fig. 4).

Identifying loss-of-function variants

Some LoF variants will result in embryonic lethality in humans in a heterozygous state, whereas others are benign even at homozygosity, with a wide spectrum of effects in between. Throughout this manuscript, we define pLoF variants to be those that introduce a premature stop (stop-gained), shift-reported transcriptional frame (frameshift), or alter the two essential splice-site nucleotides immediately to the left and right of each exon (splice) found in protein-coding transcripts, and ascertain their presence in the cohort of 125,748 individuals with exome sequence data. As these variants are enriched for annotation artefacts¹,

we developed the loss-of-function transcript effect estimator (LOFTEE) package, which applies stringent filtering criteria from first principles (such as removing terminal truncation variants, as well as rescued splice variants, that are predicted to escape nonsense-mediated decay) to pLoF variants annotated by the variant effect predictor (Extended Data Fig. 5a). Despite not using frequency information, we find that this method disproportionately removes pLoF variants that are common in the population, which are known to be enriched for annotation errors¹, while retaining rare, probable deleterious variations, as well as reported pathogenic variation (Fig. 2a). LOFTEE distinguishes high-confidence pLoF variants from annotation artefacts, and identifies a set of putative splice variants outside the essential splice site. The filtering strategy of LOFTEE is conservative in the interest of increasing specificity, filtering some potentially functional variants that display a frequency spectrum consistent with that of missense variation (Fig. 2b). Applying LOFTEE v1.0, we discover 443,769 high-confidence pLoF variants, of which 413,097 fall on the canonical transcripts of 16,694 genes. The number of pLoF variants per individual is consistent with previous reports¹, and is highly dependent on the frequency filters chosen (Supplementary Table 17).

Aggregating across variants, we created a gene-level pLoF frequency metric to estimate the proportion of haplotypes that contain an inactive

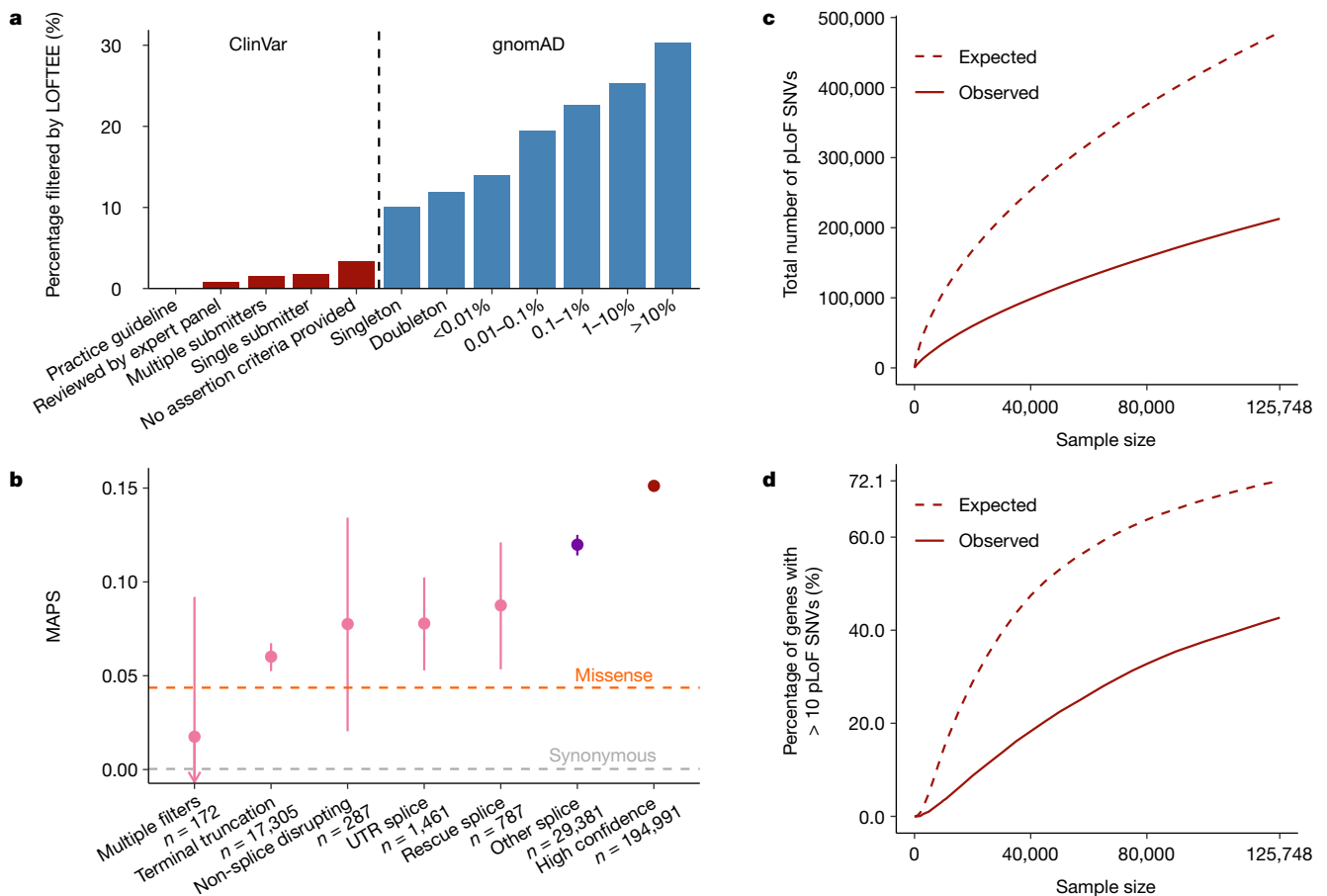


Fig. 2 | Generating a high-confidence set of pLoF variants. a, The percentage of variants filtered by LofTEE grouped by ClinVar status and gnomAD frequency. Despite not using frequency information, LofTEE removes a larger proportion of common variants, and a very low proportion of reported disease-causing variation. **b**, MAPS (see Fig. 1c, d) is shown by LofTEE designation and filter. Variants filtered out by LofTEE exhibit frequency spectra that are similar to those of missense variants; predicted splice variants outside the essential splice site are more rare, and high-confidence variants are very likely to be singletons. Only SNVs with at least 80% call rate are included

here. Error bars represent 95% confidence intervals. **c, d**, The total number of pLoF variants (**c**), and proportion of genes with more than ten pLoF variants (**d**) observed and expected (in the absence of selection) as a function of sample size (downsampled from gnomAD). Selection reduces the number of variants observed, and variant discovery approximately follows a square-root relationship with the number of samples. At current sample sizes, we would expect to identify more than 10 pLoF variants for 72.1% of genes in the absence of selection.

copy of each gene. We find that 1,555 genes have an aggregate pLoF frequency of at least 0.1% across all individuals in the dataset (Extended Data Fig. 5c), and 3,270 genes have an aggregate pLoF frequency of at least 0.1% in any one population. Furthermore, we characterized the landscape of genic tolerance to homozygous inactivation, identifying 4,332 pLoF variants that are homozygous in at least one individual. Given the rarity of true homozygous LoF variants, we expected substantial enrichment of such variants for sequencing and annotation errors, and we subjected this set to additional filtering and deep manual curation before defining a set of 1,815 genes (2,636 high-confidence variants) that are likely to be tolerant to biallelic inactivation (Supplementary Data 7).

The LoF intolerance of human genes

Just as a preponderance of pLoF variants is useful for identifying LoF-tolerant genes, we can conversely characterize the intolerance of a gene to inactivation by identifying marked depletions of predicted LoF variation^{4,7}. Here, we present a refined mutational model, which incorporates methylation, base-level coverage correction, and LofTEE (Supplementary Information, Extended Data Fig. 6), to predict expected levels of variation under neutrality. Under this updated model, the

variation in the number of synonymous variants observed is accurately captured ($r = 0.979$). We then applied this method to detect depletion of pLoF variation by comparing the number of observed pLoF variants against our expectation in the gnomAD exome data from 125,748 individuals—more than doubling the sample size of ExAC, the previously largest exome collection⁴. For this dataset, we computed a median of 17.9 expected pLoF variants per gene (Fig. 2c) and found that 72.1% of genes have more than 10 pLoF variants (powered to be classified into the most constrained genes) (Supplementary Information) expected on the canonical transcript (Fig. 2d), an increase from 13.2% and 62.8%, respectively, in ExAC.

The smaller sample size in ExAC required a transformation of the observed and expected values for the number of pLoF variants in each gene into the pLI: this metric estimates the probability that a gene falls into the class of LoF-haploinsufficient genes (approximately 10% observed/expected variation) and is ideally used as a dichotomous metric (producing 3,230 genes with pLI > 0.9). Here, our refined model and substantially increased sample size enabled us to directly assess the degree of intolerance to pLoF variation in each gene using the continuous metric of the observed/expected ratio and to estimate a confidence interval around the ratio. We find that the median observed/expected ratio is 48%, which indicates that, as noted previously, most genes

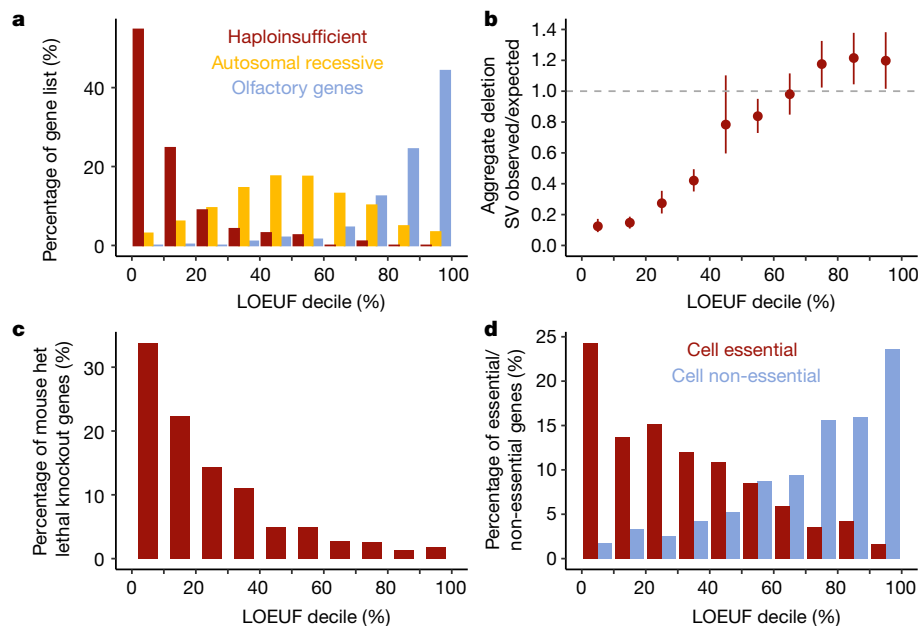


Fig. 3 | The functional spectrum of pLoF impact. **a**, The percentage of genes in a set of curated gene lists represented in each LOEUF decile. Haploinsufficient genes are enriched among the most constrained genes, whereas recessive genes are spread in the middle of the distribution, and olfactory receptor genes are largely unconstrained. **b**, The occurrence of 6,735 rare LoF deletion structural variants (SVs) is correlated with LOEUF (computed

from SNVs; linear regression $r = 0.13$; $P = 9.8 \times 10^{-68}$). Error bars represent 95% confidence intervals from bootstrapping. **c**, **d**, Constrained genes are more likely to be lethal when heterozygously inactivated in mouse and cause cellular lethality when disrupted in human cells (**c**), whereas unconstrained genes are more likely to be tolerant of disruption in cellular models (**d**). For all panels, more constrained genes are shown on the left.

exhibit at least moderate selection against pLoF variation, and that the distribution of the observed/expected ratio is not dichotomous, but continuous (Extended Data Fig. 7a). For downstream analyses, unless otherwise specified, we use the 90% upper bound of this confidence interval, which we term the loss-of-function observed/expected upper bound fraction (LOEUF) (Extended Data Fig. 7b, c), and bin 19,197 genes into deciles of approximately 1,920 genes each. At current sample sizes, this metric enables the quantitative assessment of constraint with a built-in confidence value, and distinguishes small genes (for example, those with observed = 0, expected = 2; LOEUF = 1.34) from large genes (for example, observed = 0, expected = 100; LOEUF = 0.03), while retaining the continuous properties of the direct estimate of the ratio (Supplementary Information). At one extreme of the distribution, we observe genes with a very strong depletion of pLoF variation (first LOEUF decile aggregate observed/expected approximately 6%) (Extended Data Fig. 7e), including genes previously characterized as high pLI (Extended Data Fig. 7f). By contrast, we find unconstrained genes that are relatively tolerant of inactivation, including many that contain homozygous pLoF variants (Extended Data Fig. 7g).

We note that the use of the upper bound means that LOEUF is a conservative metric in one direction: genes with low LOEUF scores are confidently depleted for pLoF variation, whereas genes with high LOEUF scores are a mixture of genes without depletion, and genes that are too small to obtain a precise estimate of the observed/expected ratio. In general, however, the scale of gnomAD means that gene length is rarely a substantive confounder for the analyses described here, and all downstream analyses are adjusted for the length of the coding sequence or filtered to genes with at least ten expected pLoFs (Supplementary Information).

Validation of the LoF-intolerance score

The LOEUF metric allows us to place each gene along a continuous spectrum of tolerance to inactivation. We examined the correlation of

this metric with several independent measures of genic sensitivity to disruption. First, we found that LOEUF is consistent with the expected behaviour of well-established gene sets: known haploinsufficient genes are strongly depleted of pLoF variation, whereas olfactory receptors are relatively unconstrained, and genes with a known autosomal recessive mechanism, for which selection against heterozygous disruptive variants tends to be present but weak⁹, fall in the middle of the distribution (Fig. 3a). In addition, LOEUF is positively correlated with the occurrence of 6,735 rare autosomal deletion structural variants overlapping protein-coding exons identified in a subset of 6,749 individuals with whole-genome sequencing data in this manuscript¹¹ ($r = 0.13$; $P = 9.8 \times 10^{-68}$) (Fig. 3b).

This constraint metric also correlates with results in model systems: in 389 genes with orthologues that are embryonically lethal after heterozygous deletion in mouse^{21,22}, we find a lower LOEUF score (mean = 0.488), compared with the remaining 18,808 genes (mean = 0.962; t -test $P = 10^{-78}$) (Fig. 3c). Similarly, the 678 genes that are essential for human cell viability as characterized by CRISPR screens²³ are also depleted for pLoF variation (mean LOEUF = 0.63) in the general population compared to background (18,519 genes with mean LOEUF = 0.964; t -test $P = 9 \times 10^{-71}$), whereas the 777 non-essential genes are more likely to be unconstrained (mean LOEUF = 1.34, compared to remaining 18,420 genes with mean LOEUF = 0.936; t -test $P = 3 \times 10^{-92}$) (Fig. 3d).

Biological properties of constraint

We investigated the properties of genes and transcripts as a function of their tolerance to pLoF variation (LOEUF). First, we found that LOEUF correlates with the degree of connection of a gene in protein-interaction networks ($r = -0.14$; $P = 1.7 \times 10^{-51}$ after adjusting for gene length) (Fig. 4a) and functional characterization (Extended Data Fig. 8a). In addition, constrained genes are more likely to be ubiquitously expressed across 38 tissues in the Genotype-Tissue Expression

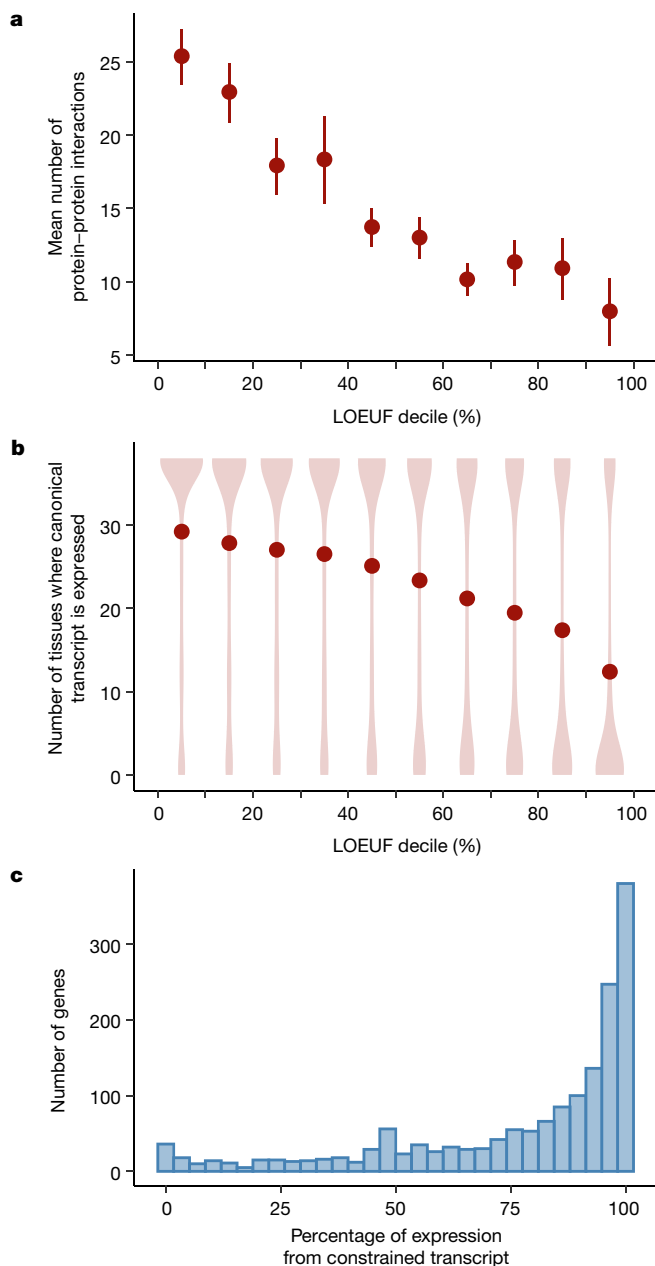


Fig. 4 | Biological properties of constrained genes and transcripts. **a**, The mean number of protein-protein interactions is plotted as a function of LOEUF decile: more constrained genes have more interaction partners (LOEUF linear regression $r = -0.14$; $P = 1.7 \times 10^{-51}$). Error bars correspond to 95% confidence intervals. **b**, The number of tissues where a gene is expressed (transcripts per million > 0.3), binned by LOEUF decile, is shown as a violin plot with the mean number overlaid as points: more constrained genes are more likely to be expressed in several tissues (LOEUF linear regression $r = -0.31$; $P < 1 \times 10^{-100}$). **c**, For 1,740 genes in which there exists at least one constrained and one unconstrained transcript, the proportion of expression derived from the constrained transcript is plotted as a histogram.

(GTEx) project (Fig. 4b) (LOEUF $r = -0.31$; $P < 1 \times 10^{-100}$) and have higher expression on average (LOEUF $\rho = -0.28$; $P < 1 \times 10^{-100}$), consistent with previous results⁴. Although most results in this study are reported at the gene level, we have also extended our framework to compute LOEUF for all protein-coding transcripts, allowing us to explore the extent of differential constraint of transcripts within a given gene. In cases in which a gene contained transcripts with varying levels of constraint, we

found that transcripts in the first LOEUF decile were more likely to be expressed across tissues than others in the same gene ($n = 1,740$ genes), even when adjusted for transcript length (Fig. 4c) (constrained transcripts are on average 6.34 transcripts per million higher; $P = 2.2 \times 10^{-14}$). Furthermore, we found that the most constrained transcript for each gene was typically the most highly expressed transcript in tissues with disease relevance²⁴ (Extended Data Fig. 8c), which supports the need for transcript-based variant interpretation, as explored in more depth in an accompanying manuscript¹⁵.

Finally, we investigated potential differences in LOEUF across human populations, restricting to the same sample size across all populations to remove bias due to differential power for variant discovery. As the smallest population in our exome dataset (African/African American) has only 8,128 individuals, our ability to detect constraint against pLoF variants for individual genes is limited. However, for well-powered genes (expected pLoF ≥ 10) (Supplementary Information), we observed a lower mean observed/expected ratio and LOEUF across genes among African/African American individuals, a population with a larger effective population size, compared with other populations (Extended Data Fig. 8d, e), consistent with the increased efficiency of selection in populations with larger effective population sizes^{25,26}.

Constraint informs disease aetiologies

The LOEUF metric can be applied to improve molecular diagnosis and advance our understanding of disease mechanisms. Disease-associated genes, discovered by different technologies over the course of many years across all categories of inheritance and effects, span the entire spectrum of LoF tolerance (Extended Data Fig. 9a). However, in recent years, high-throughput sequencing technologies have enabled the identification of highly deleterious variants that are de novo or only inherited in small families or trios, leading to the discovery of novel disease genes under extreme constraint against pLoF variation that could not have been identified by linkage approaches that rely on broadly inherited variation (Extended Data Fig. 9b). This result is consistent with a recent analysis that shows a post-whole-exome/whole-genome sequencing era enrichment for gene-disease relationships attributable to de novo variants²⁷.

Rare variants, which are more likely to be deleterious, are expected to exhibit stronger effects on average in constrained genes (previously shown using pLI from ExAC²⁸), with an effect size related to the severity and reproductive fitness of the phenotype. In an independent cohort of 5,305 individuals with intellectual disability or developmental disorders and 2,179 controls, the rate of pLoF de novo variation in cases is 15-fold higher in genes belonging to the most constrained LOEUF decile, compared with controls (Fig. 5a), with a slightly increased rate (2.9-fold) in the second highest decile but not in others. A similar, but attenuated enrichment (4.4-fold in the most constrained decile) is seen for de novo variants in 6,430 patients with autism spectrum disorder (Extended Data Fig. 9c). Furthermore, in burden tests of rare variants (allele count across both cases and controls = 1) of patients with schizophrenia²⁸, we find a significantly higher odds ratio in constrained genes (Extended Data Fig. 9d).

Finally, although pLoF variants are predominantly rare, other more common variation in constrained genes may also be deleterious, including the effects of other coding or regulatory variants. In a heritability partitioning analysis of association results for 658 traits in the UK Biobank and other large-scale genome-wide association study (GWAS) efforts, we find an enrichment of common variant associations near genes that is linearly related to LOEUF decile across numerous traits (Fig. 5b). Schizophrenia and educational attainment are the most enriched traits (Fig. 5c), consistent with previous observations in associations between rare pLoF variants and these phenotypes²⁹⁻³¹. This enrichment persists even when accounting for gene size, expression in GTEx brain samples, and previously tested annotations of functional

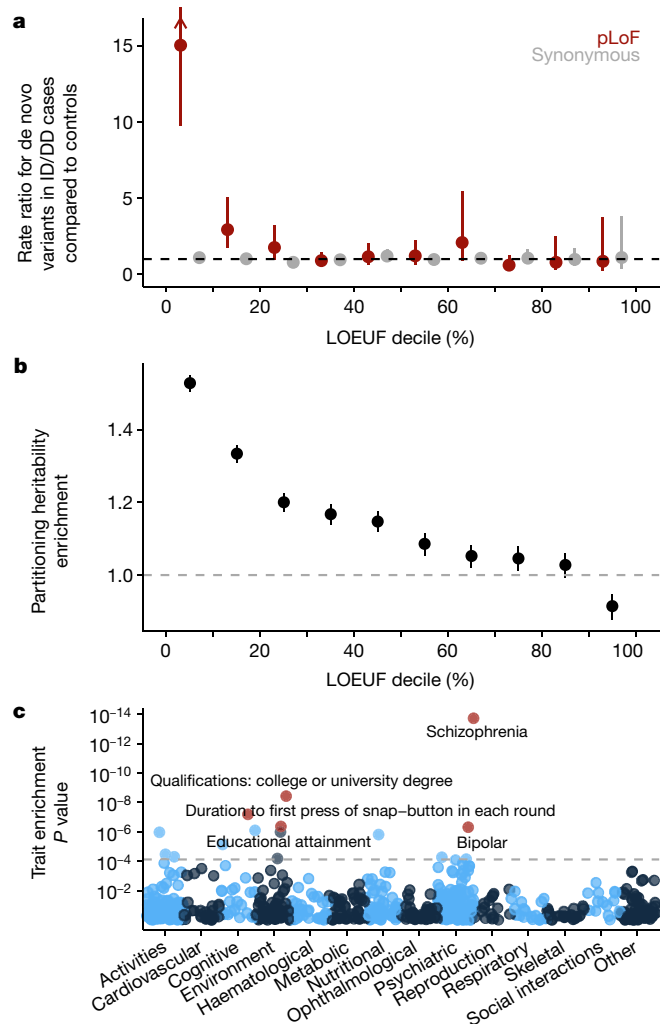


Fig. 5 | Disease applications of constraint. a, The rate ratio is defined by the rate of de novo variants (number per patient) in 5,305 cases of intellectual disability/developmental delay (ID/DD) divided by the rate in 2,179 controls. pLoF variants in the most constrained decile of the genome are approximately 11-fold more likely to be found in cases compared to controls. Error bars represent 95% confidence intervals. **b,** Marginal enrichment in per-SNV heritability explained by common (minor allele frequency > 5%) variants within 100-kb of genes in each LOEUF decile, estimated by linkage disequilibrium (LD) score regression⁴⁸. Enrichment is compared to the average SNV genome-wide. The results reported here are from random effects meta-analysis of 276 independent traits (subsampled from the 658 traits with UK Biobank or large-scale consortium GWAS results). Error bars represent 95% confidence intervals. **c,** Conditional enrichment in per-SNV common variant heritability tested using regression of linkage disequilibrium score in each of 658 common disease and trait GWAS results. P values evaluate whether per-SNV heritability is proportional to the LOEUF of the nearest gene, conditional on 75 existing functional, linkage disequilibrium, and minor-allele-frequency-related genomic annotations. Colours alternate by broad phenotype category.

regions and evolutionary conservation, and suggests that some heritable polygenic diseases and traits, particularly cognitive or psychiatric ones, have an underlying genetic architecture that is driven substantially by constrained genes (Extended Data Fig. 10).

Discussion

In this paper and accompanying publications, we present the largest, to our knowledge, catalogue of harmonized variant data from any species so far, incorporating exome or genome sequence data from

more than 140,000 humans. The gnomAD dataset of over 270 million variants is publicly available (<https://gnomad.broadinstitute.org>), and has already been widely used as a resource for estimates of allele frequency in the context of rare disease diagnosis (for a recent review, see Eilbeck et al.³²), improving power for disease gene discovery^{33–35}, estimating genetic disease frequencies^{36,37}, and exploring the biological effect of genetic variation^{38,39}. Here, we describe the application of this dataset to calculate a continuous metric that describes a spectrum of tolerance to pLoF variation for each protein-coding gene in the human genome. We validate this method using known gene sets and data from model organisms, and explore the value of this metric for investigating human gene function and discovery of disease genes.

We have focused on high-confidence, high-impact pLoF variants, calibrating our analysis to be highly specific to compensate for the increased false-positive rate among deleterious variants. However, some additional error modes may still exist, and indeed, several recent experiments have proposed uncharacterized mechanisms for escape from nonsense-mediated mRNA decay^{40,41}. Furthermore, such a stringent approach will remove some true positives. For example, terminal truncations that are removed by LOFTEE may still exert a LoF mechanism through the removal of crucial C-terminal domains, despite the escape of the gene from nonsense-mediated decay. In addition, current annotation tools are incapable of detecting all classes of LoF variation and typically miss, for instance, missense variants that inactivate specific gene functions, as well as high-impact variants in regulatory regions. Future work will benefit from the increasing availability of high-throughput experimental assays that can assess the functional effect of all possible coding variants in a target gene⁴², although scaling these experimental assays to all protein-coding genes represents a huge challenge. Identifying constraint in individual regulatory elements outside coding regions will be even more challenging, and require much larger sample sizes of whole genomes as well as improved functional annotation⁴³. We discuss one class of high-impact regulatory variants in a companion manuscript¹⁷, but many remain to be fully characterized.

Although the gnomAD dataset is of unprecedented scale, it has important limitations. At this sample size, we remain far from saturating all possible pLoF variants in the human exome; even at the most mutable sites in the genome (methylated CpG dinucleotides), we observe only half of all possible stop-gained variants. A substantial fraction of the remaining variants are likely to be heterozygous lethal, whereas others will exhibit an intermediate selection coefficient; much larger sample sizes (in the millions to hundreds of millions of individuals) will be required for comprehensive characterization of selection against all individual LoF variants in the human genome. Such future studies would also benefit substantially from increased ancestral diversity beyond the European-centric sampling of many current studies, which would provide opportunities to observe very rare and population-specific variation, as well as increase power to explore population differences in gene constraint. In particular, current reference databases including gnomAD have a near-complete absence of representation from the Middle East, central and southeast Asia, Oceania, and the vast majority of the African continent⁴⁴, and these gaps must be addressed if we are to fully understand the distribution and effect of human genetic variation.

It is also important to understand the practical and evolutionary interpretation of pLoF constraint. In particular, it should be noted that these metrics primarily identify genes undergoing selection against heterozygous variation, rather than strong constraint against homozygous variation⁴⁵. In addition, the power of the LOEUF metric is affected by gene length, with approximately 30% of the coding genes in the genome still insufficiently powered for detection of constraint even at the scale of gnomAD (Fig. 2d). Substantially larger sample sizes and careful analysis of individuals enriched for homozygous pLoFs (see below) will be useful for distinguishing these possibilities. Furthermore, selection is largely blind to phenotypes emerging after reproductive age, and thus genes with phenotypes that manifest later in life, even if

severe or fatal, may exhibit much weaker intolerance to inactivation. Despite these caveats, our results demonstrate that pLoF constraint divides protein-coding genes in a way that correlates usefully with their probability of disease impact and other biological properties, and confirm the value of constraint in prioritizing candidate genes in studies of both rare and common diseases.

Examples such as *PCSK9* demonstrate the value of human pLoF variants for identifying and validating targets for therapeutic intervention across a wide range of human diseases. As discussed in more detail in an accompanying manuscript¹², careful attention must be paid to a variety of complicating factors when using pLoF constraint to assess candidates. More valuable information comes from directly exploring the phenotypic effect of LoF variants on carrier humans, both through ‘forward genetics’ approaches such as gene mapping to identify genes that cause Mendelian disease, as well as ‘reverse genetics’ approaches that leverage large collections of sequenced humans to find and clinically characterize individuals with disruptive mutations in specific genes. Although clinical data are currently available for only a small subset of gnomAD individuals, future efforts that integrate sequencing and deep phenotyping of large biobanks will provide valuable insight into the biological implications of partial disruption of specific genes. This is illustrated in a companion manuscript that explores the clinical correlates of heterozygous pLoF variants in the *LRRK2* gene, demonstrating that life-long partial inactivation of this gene is likely to be safe in humans¹³.

Such examples, and the sheer scale of pLoF discovery in this dataset, suggest the near-future feasibility and considerable value of a human ‘knockout’ project—a systematic attempt to discover the phenotypic consequences of functionally disruptive mutations, in either the heterozygous or homozygous state, for all human protein-coding genes. Such an approach will require cohorts of samples from millions of sequenced and deeply, consistently phenotyped individuals and, for the discovery of ‘complete’ knockouts, would benefit substantially from the targeted inclusion of large numbers of samples from populations that have either experienced strong demographic bottlenecks or high levels of recent parental relatedness (consanguinity)¹². Such a resource would allow the construction of a comprehensive map that directly links gene-disrupting variation to human biology.

Online content

Any methods, additional references, Nature Research reporting summaries, source data, extended data, supplementary information, acknowledgements, peer review information; details of author contributions and competing interests; and statements of data and code availability are available at <https://doi.org/10.1038/s41586-020-2308-7>.

1. MacArthur, D. G. et al. A systematic survey of loss-of-function variants in human protein-coding genes. *Science* **335**, 823–828 (2012).
2. Schneeberger, K. Using next-generation sequencing to isolate mutant genes from forward genetic screens. *Nat. Rev. Genet.* **15**, 662–676 (2014).
3. Zambrowicz, B. P. & Sands, A. T. Knockouts model the 100 best-selling drugs—will they model the next 100? *Nat. Rev. Drug Discov.* **2**, 38–51 (2003).
4. Lek, M. et al. Analysis of protein-coding genetic variation in 60,706 humans. *Nature* **536**, 285–291 (2016).
5. Chong, J. X. et al. The genetic basis of mendelian phenotypes: discoveries, challenges, and opportunities. *Am. J. Hum. Genet.* **97**, 199–215 (2015).
6. Cohen, J. C., Boerwinkle, E., Mosley, T. H., Jr & Hobbs, H. H. Sequence variations in *PCSK9*, low LDL, and protection against coronary heart disease. *N. Engl. J. Med.* **354**, 1264–1272 (2006).
7. Samocha, K. E. et al. A framework for the interpretation of de novo mutation in human disease. *Nat. Genet.* **46**, 944–950 (2014).
8. Petrovski, S., Wang, Q., Heinzen, E. L., Allen, A. S. & Goldstein, D. B. Genic intolerance to functional variation and the interpretation of personal genomes. *PLoS Genet.* **9**, e1003709 (2013).
9. Cassa, C. A. et al. Estimating the selective effects of heterozygous protein-truncating variants from human exome data. *Nat. Genet.* **49**, 806–810 (2017).
10. Petrovski, S. et al. The intolerance of regulatory sequence to genetic variation predicts gene dosage sensitivity. *PLoS Genet.* **11**, e1005492 (2015).
11. Collins, R. L. et al. A structural variation reference for medical and population genetics. *Nature* <https://doi.org/10.1038/s41586-020-2287-8> (2020).
12. Minikel, E. V. et al. Evaluating drug targets through human loss-of-function genetic variation. *Nature* <https://doi.org/10.1038/s41586-020-2267-z> (2020).

13. Whiffin, N. et al. The effect of *LRRK2* loss-of-function variants in humans. *Nature Med.* <https://doi.org/10.1038/s41591-020-0893-5> (2020).
14. GTEx Consortium. Genetic effects on gene expression across human tissues. *Nature* **550**, 204–213 (2017).
15. Cummings, B. B. et al. Transcript expression-aware annotation improves rare variant interpretation. *Nature* <https://doi.org/10.1038/s41586-020-2329-2> (2020).
16. Wang, Q. et al. Landscape of multi-nucleotide variants in 125,748 human exomes and 15,708 genomes. *Nat. Commun.* <https://doi.org/10.1038/s41467-019-12438-5> (2020).
17. Whiffin, N. et al. Characterising the loss-of-function impact of 5' untranslated region variants in whole genome sequence data from 15,708 individuals. *Nat. Commun.* <https://doi.org/10.1038/s41467-019-10717-9> (2019).
18. Van der Auwera, G. A. et al. From FastQ data to high confidence variant calls: the Genome Analysis Toolkit best practices pipeline. *Curr. Protoc. Bioinformatics* **43**, 11.10.1–11.19.33 (2013).
19. Hail Team. Hail 0.2.19; <https://github.com/hail-is/hail/releases/tag/0.2.19> (released 2 August 2019).
20. Jónsson, H. et al. Parental influence on human germline de novo mutations in 1,548 trios from Iceland. *Nature* **549**, 519–522 (2017).
21. Motenko, H., Neuhauser, S. B., O’Keefe, M. & Richardson, J. E. MouseMine: a new data warehouse for MGI. *Mamm. Genome* **26**, 325–330 (2015).
22. Eppig, J. T., Blake, J. A., Bult, C. J., Kadin, J. A. & Richardson, J. E. The Mouse Genome Database (MGD): facilitating mouse as a model for human biology and disease. *Nucleic Acids Res.* **43**, D726–D736 (2015).
23. Hart, T. et al. Evaluation and design of genome-wide CRISPR/SpCas9 knockout screens. *G3 (Bethesda)* **7**, 2719–2727 (2017).
24. Feiglin, A., Allen, B. K., Kohane, I. S. & Kong, S. W. Comprehensive analysis of tissue-wide gene expression and phenotype data reveals tissues affected in rare genetic disorders. *Cell Syst.* **5**, 140–148.e2 (2017).
25. Gravel, S. When is selection effective? *Genetics* **203**, 451–462 (2016).
26. Henn, B. M., Botigué, L. R., Bustamante, C. D., Clark, A. G. & Gravel, S. Estimating the mutation load in human genomes. *Nat. Rev. Genet.* **16**, 333–343 (2015).
27. Bamshad, M. J., Nickerson, D. A. & Chong, J. X. mendelian gene discovery: fast and furious with no end in sight. *Am. J. Hum. Genet.* **105**, 448–455 (2019).
28. Walters, J. T. R. et al. The contribution of rare variants to risk of schizophrenia in individuals with and without intellectual disability. *Nat. Genet.* **51**, 421 (2017).
29. Ganna, A. et al. Quantifying the impact of rare and ultra-rare coding variation across the phenotypic spectrum. *Am. J. Hum. Genet.* **102**, 1204–1211 (2018).
30. Ganna, A. et al. Ultra-rare disruptive and damaging mutations influence educational attainment in the general population. *Nat. Neurosci.* **19**, 1563–1565 (2016).
31. Genovese, G. et al. Increased burden of ultra-rare protein-altering variants among 4,877 individuals with schizophrenia. *Nat. Neurosci.* **19**, 1433–1441 (2016).
32. Eilbeck, K., Quinlan, A. & Yandell, M. Settling the score: variant prioritization and Mendelian disease. *Nat. Rev. Genet.* **18**, 599–612 (2017).
33. DeBoever, C. et al. Medical relevance of protein-truncating variants across 337,205 individuals in the UK Biobank study. *Nat. Commun.* **9**, 1612 (2018).
34. Emdin, C. A. et al. Analysis of predicted loss-of-function variants in UK Biobank identifies variants protective for disease. *Nat. Commun.* **9**, 1613 (2018).
35. Satterstrom, F. K. et al. Autism spectrum disorder and attention deficit hyperactivity disorder have a similar burden of rare protein-truncating variants. *Nat. Neurosci.* **22**, 1961–1965 (2019).
36. de Andrade, K. C. et al. Variable population prevalence estimates of germline TP53 variants: a gnomAD-based analysis. *Hum. Mutat.* **40**, 97–105 (2019).
37. Laver, T. W. et al. Analysis of large-scale sequencing cohorts does not support the role of variants in UCP2 as a cause of hyperinsulinaemic hypoglycaemia. *Hum. Mutat.* **38**, 1442–1444 (2017).
38. Sundaram, L. et al. Predicting the clinical impact of human mutation with deep neural networks. *Nat. Genet.* **50**, 1161–1170 (2018).
39. Glassberg, E. C., Lan, X. & Pritchard, J. K. Evidence for weak selective constraint on human gene expression. *Genetics* **211**, 757–772 (2019).
40. El-Brolosy, M. A. et al. Genetic compensation triggered by mutant mRNA degradation. *Nature* **568**, 193–197 (2019).
41. Tuladhar, R. et al. CRISPR-Cas9-based mutagenesis frequently provokes on-target mRNA misregulation. *Nat. Commun.* **10**, 4056 (2019).
42. Findlay, G. M. et al. Accurate classification of *BRCA1* variants with saturation genome editing. *Nature* **562**, 217–222 (2018).
43. Short, P. J. et al. De novo mutations in regulatory elements in neurodevelopmental disorders. *Nature* **555**, 611–616 (2018).
44. Martin, A. R., Kanai, M., Kamatani, Y., Neale, B. M. & Daly, M. J. Hidden ‘risk’ in polygenic scores: clinical use today could exacerbate health disparities. *Nat. Genet.* **51**, 584–591 (2019).
45. Fuller, Z., Berg, J. J., Mostafavi, H., Sella, G. & Przeworski, M. Measuring intolerance to mutation in human genetics. *Nat. Genet.* **51**, 772–776 (2019).
46. McInnes, L., Healy, J., Saul, N. & Großberger, L. UMAP: Uniform Manifold Approximation and Projection. *J. Open Source Softw.* **3**, 861 (2018).
47. Diaz-Papkovich, A., Anderson-Trocme, L. & Gravel, S. UMAP reveals cryptic population structure and phenotype heterogeneity in large genomic cohorts. *PLoS Genet.* (2018). <https://doi.org/10.1371/journal.pgen.1008432>
48. Finucane, H. K. Partitioning heritability by functional annotation using genome-wide association summary statistics. *Nat. Genet.* **47**, 1228–1235 (2015).
49. Zook, J. M. et al. Integrating human sequence data sets provides a resource of benchmark SNP and indel genotype calls. *Nat. Biotechnol.* **32**, 246–251 (2014).
50. Li, H. et al. A synthetic-diploid benchmark for accurate variant-calling evaluation. *Nat. Methods* **15**, 595–597 (2018).
51. Fromer, M. et al. De novo mutations in schizophrenia implicate synaptic networks. *Nature* **506**, 179–184 (2014).
52. Neale, B. M. et al. Patterns and rates of exonic de novo mutations in autism spectrum disorders. *Nature* **485**, 242–245 (2012).

Publisher's note Springer Nature remains neutral with regard to jurisdictional claims in published maps and institutional affiliations.



Open Access This article is licensed under a Creative Commons Attribution 4.0 International License, which permits use, sharing, adaptation, distribution and reproduction in any medium or format, as long as you give appropriate credit to the original author(s) and the source, provide a link to the Creative Commons license, and indicate if changes were made. The images or other third party material in this article are included in the article's Creative Commons license, unless indicated otherwise in a credit line to the material. If material is not included in the article's Creative Commons license and your intended use is not permitted by statutory regulation or exceeds the permitted use, you will need to obtain permission directly from the copyright holder. To view a copy of this license, visit <http://creativecommons.org/licenses/by/4.0/>.

© The Author(s) 2020

Genome Aggregation Database Consortium

Carlos A. Aguilar Salinas²⁰, Tariq Ahmad²¹, Christine M. Albert^{22,23}, Diego Ardissino²⁴, Gil Atzmon^{25,26,27}, John Barnard²⁸, Laurent Beaugier²⁹, Emelia J. Benjamin^{30,31,32}, Michael Boehnke³³, Lori L. Bonycastle³⁴, Erwin P. Bottinger³⁵, Donald W. Bowden^{36,37,38}, Matthew J. Bown^{39,40}, John C. Chambers^{41,42,43}, Juliana C. Chan⁴⁴, Daniel Chasman^{22,45}, Judy Cho³⁵, Mina K. Chung²⁸, Bruce Cohen^{45,46}, Adolfo Correa⁴⁷, Dana Dabelea⁴⁸, Mark J. Daly^{12,9}, Dawood Darbar⁴⁹, Ravindranath Duggirala⁵⁰, Josée Dupuis^{30,51}, Patrick T. Ellinor^{1,52}, Roberto Elosua^{53,54,55}, Jeanette Erdmann^{56,57,58}, Tõnu Esko^{1,59}, Martti Färkkilä⁶⁰, Jose Florez^{1,7,61,62,63}, Andre Franke⁶⁴, Gad Getz^{45,65,66,67,68}, Benjamin Glaser⁶⁹, Stephen J. Glatt⁷⁰, David Goldstein^{71,72}, Clicerio Gonzalez⁷³, Leif Groop^{6,74}, Christopher Haiman⁷⁵, Craig Hanis⁷⁶, Matthew Harms^{77,78}, Mikko Hiltunen⁷⁹, Matti M. Holi⁸⁰, Christina M. Hultman^{81,82}, Mikko Kallela⁸³, Jaakko Kaprio⁸⁴, Sekar Kathiresan^{5,45,85}, Bong-Jo Kim⁸⁶, Young Jin Kim⁸⁶, George Kirov⁸⁷, Jaspal Kooner^{10,41,42,43}, Seppo Koskinen⁸⁸, Harlan M. Krumholz⁸⁹, Subra Kugathasan⁹⁰, Soo Heon Kwak⁹¹, Markku Laakso^{92,93}, Terho Lehtimäki⁹⁴, Ruth J. F. Loos^{35,95}, Steven A. Lubitz^{1,52}, Ronald C. W. Ma^{44,96,97}, Daniel G. MacArthur^{1,2}, Jaume Marrugat^{54,98}, Kari M. Mattila⁹⁴, Steven McCarroll^{9,99}, Mark I. McCarthy^{100,101,102}, Dermot McGovern¹⁰³, Ruth McPherson¹⁰⁴, James B. Meigs^{1,45,105}, Olle Melander¹⁰⁶, Andres Metspalu⁵⁹, Benjamin M. Neale^{1,2}, Peter M. Nilsson¹⁰⁷, Michael C. O'Donovan⁸⁷, Dost Ongur^{45,46}, Lorena Orozco¹⁰⁸, Michael J. Owen⁸⁷, Colin N. A. Palmer¹⁰⁹, Aarno Palotie^{1,6,9}, Kyong Soo Park^{91,110}, Carlos Pato¹¹¹, Ann E. Pulver¹¹², Nazneen Rahman¹¹³, Anne M. Remes¹¹⁴, John D. Rioux^{115,116}, Samuli Ripatti^{1,6,84}, Dan M. Roden^{117,118}, Danish Saleheen^{119,120,121}, Veikko Salomaa¹²², Nilesh J. Samani^{39,40}, Jeremiah Scharf^{1,5,9}, Heribert Schunkert^{123,124}, Moore B. Shoemaker¹²⁵, Pamela Sklar^{62,126,127,128,151}, Hilikka Soininen¹²⁹, Harry Sokol¹²⁹, Tim Spector¹³⁰, Patrick F. Sullivan^{81,131}, Jaana Suvisaari¹²², E. Shyong Tai^{132,133,134}, Yik Ying Teo^{132,135,136}, Tuomi Tiiamaaija^{6,137,138}, Ming Tsuang^{139,140}, Dan Turner¹⁴¹, Teresa Tusie-Luna^{142,143}, Erkki Vartiainen⁸⁴, James S. Ware^{130,11}, Hugh Watkins¹⁴⁴, Rinse K. Weersma¹⁴⁵, Maija Wessman^{6,137}, James G. Wilson¹⁴⁶ & Rannik J. Xavier^{147,148}

²⁰Unidad de Investigación de Enfermedades Metabólicas, Instituto Nacional de Ciencias Medicas y Nutrición, Mexico City, Mexico. ²¹Peninsula College of Medicine and Dentistry, Exeter, UK. ²²Division of Preventive Medicine, Brigham and Women's Hospital, Boston, MA, USA. ²³Division of Cardiovascular Medicine, Brigham and Women's Hospital and Harvard Medical School, Boston, MA, USA. ²⁴Department of Cardiology, University Hospital, Parma, Italy. ²⁵Department of Biology, Faculty of Natural Sciences, University of Haifa, Haifa, Israel. ²⁶Department of Medicine, Albert Einstein College of Medicine, Bronx, NY, USA. ²⁷Department of Genetics, Albert Einstein College of Medicine, Bronx, NY, USA. ²⁸Department of Quantitative Health Sciences, Lerner Research Institute, Cleveland Clinic, Cleveland, OH, USA. ²⁹Sorbonne Université, APHP, Gastroenterology Department, Saint Antoine Hospital, Paris, France. ³⁰Framingham Heart Study, National Heart, Lung, & Blood Institute and Boston University, Framingham, MA, USA. ³¹Department of Medicine, Boston University School of Medicine, Boston, MA, USA. ³²Department of Epidemiology, Boston University School of Public Health, Boston, MA, USA. ³³Department of Biostatistics, Center for Statistical Genetics, University of Michigan, Ann Arbor, MI, USA. ³⁴National Human Genome Research Institute, National Institutes of Health, Bethesda, MD, USA. ³⁵The Charles Bronfman Institute for Personalized Medicine, Icahn School of Medicine at Mount Sinai, New York, NY, USA. ³⁶Department of Biochemistry, Wake Forest School of Medicine, Winston-Salem, NC, USA. ³⁷Center for Genomics and Personalized Medicine Research, Wake Forest School of Medicine, Winston-Salem, NC, USA. ³⁸Center for Diabetes Research, Wake Forest School of Medicine, Winston-Salem, NC, USA. ³⁹Department of Cardiovascular Sciences and NIHR Leicester Biomedical Research Centre, University of Leicester, Leicester, UK. ⁴⁰NIHR Leicester Biomedical Research Centre, Glenfield Hospital, Leicester, UK. ⁴¹Department of Epidemiology and Biostatistics, Imperial College London, London, UK. ⁴²Department of Cardiology, Ealing Hospital NHS Trust, Southall, UK. ⁴³Imperial College Healthcare NHS Trust, Imperial College London, London, UK. ⁴⁴Department of Medicine and Therapeutics, The Chinese University of Hong Kong, Hong Kong, China. ⁴⁵Department of Medicine, Harvard Medical School, Boston, MA, USA. ⁴⁶Program for Neuropsychiatric Research, McLean Hospital, Belmont, MA, USA. ⁴⁷Department of Medicine, University of Mississippi Medical Center, Jackson, MI, USA. ⁴⁸Department of Epidemiology, Colorado School of Public Health, Aurora, CO, USA. ⁴⁹Department of Medicine and Pharmacology, University of Illinois at Chicago, Chicago, IL,

USA. ⁵⁰Department of Genetics, Texas Biomedical Research Institute, San Antonio, TX, USA. ⁵¹Department of Biostatistics, Boston University School of Public Health, Boston, MA, USA. ⁵²Cardiac Arrhythmia Service and Cardiovascular Research Center, Massachusetts General Hospital, Boston, MA, USA. ⁵³Cardiovascular Epidemiology and Genetics, Hospital del Mar Medical Research Institute (IMIM), Barcelona, Catalonia, Spain. ⁵⁴Centro de Investigación Biomédica en Red Enfermedades Cardiovasculares (CIBERCV), Barcelona, Catalonia, Spain. ⁵⁵Department of Medicine, Medical School, University of Vic-Central University of Catalonia, Vic, Catalonia, Spain. ⁵⁶Institute for Cardiogenetics, University of Lübeck, Lübeck, Germany. ⁵⁷DZHK (German Research Centre for Cardiovascular Research), partner site Hamburg/Lübeck/Kiel, Lübeck, Germany. ⁵⁸University Heart Center Lübeck, Lübeck, Germany. ⁵⁹Estonian Genome Center, Institute of Genomics, University of Tartu, Tartu, Estonia. ⁶⁰Helsinki University and Helsinki University Hospital, Clinic of Gastroenterology, Helsinki, Finland. ⁶¹Diabetes Unit, Massachusetts General Hospital, Boston, MA, USA. ⁶²Center for Genomic Medicine, Massachusetts General Hospital, Boston, MA, USA. ⁶³Program in Metabolism, Broad Institute of MIT and Harvard, Cambridge, MA, USA. ⁶⁴Institute of Clinical Molecular Biology (IKMB), Christian-Albrechts-University of Kiel, Kiel, Germany. ⁶⁵Bioinformatics Consortium, Massachusetts General Hospital, Boston, MA, USA. ⁶⁶Cancer Genome Computational Analysis Group, Broad Institute of MIT and Harvard, Cambridge, MA, USA. ⁶⁷Department of Pathology, Massachusetts General Hospital, Boston, MA, USA. ⁶⁸Cancer Center, Massachusetts General Hospital, Boston, MA, USA. ⁶⁹Endocrinology and Metabolism Department, Hadassah-Hebrew University Medical Center, Jerusalem, Israel. ⁷⁰Department of Psychiatry and Behavioral Sciences, SUNY Upstate Medical University, Syracuse, NY, USA. ⁷¹Institute for Genomic Medicine, Columbia University Medical Center, Hammer Health Sciences, New York, NY, USA. ⁷²Department of Genetics and Development, Columbia University Medical Center, Hammer Health Sciences, New York, NY, USA. ⁷³Centro de Investigación en Salud Poblacional, Instituto Nacional de Salud Pública, Cuernavaca, Mexico. ⁷⁴Genomics, Diabetes and Endocrinology, Lund University, Lund, Sweden. ⁷⁵Lund University Diabetes Centre, Malmö, Sweden. ⁷⁶Human Genetics Center, University of Texas Health Science Center at Houston, Houston, TX, USA. ⁷⁷Department of Neurology, Columbia University, New York, NY, USA. ⁷⁸Institute of Genomic Medicine, Columbia University, New York, NY, USA. ⁷⁹Institute of Biomedicine, University of Eastern Finland, Kuopio, Finland. ⁸⁰Department of Psychiatry, Helsinki University Central Hospital, Lapinlahdentie, Helsinki, Finland. ⁸¹Department of Medical Epidemiology and Biostatistics, Karolinska Institutet, Stockholm, Sweden. ⁸²Icahn School of Medicine at Mount Sinai, New York, NY, USA. ⁸³Department of Neurology, Helsinki University Central Hospital, Helsinki, Finland. ⁸⁴Department of Public Health, Faculty of Medicine, University of Helsinki, Helsinki, Finland. ⁸⁵Cardiovascular Disease Initiative and Program in Medical and Population Genetics, Broad Institute of MIT and Harvard, Cambridge, MA, USA. ⁸⁶Center for Genome Science, Korea National Institute of Health, Chungcheongbuk-do, South Korea. ⁸⁷MRC Centre for Neuropsychiatric Genetics & Genomics, Cardiff University School of Medicine, Cardiff, UK. ⁸⁸Department of Health, National Institute for Health and Welfare (THL), Helsinki, Finland. ⁸⁹Section of Cardiovascular Medicine, Department of Internal Medicine, Yale School of Medicine, New Haven, CT, USA. ⁹⁰Division of Pediatric Gastroenterology, Emory University School of Medicine, Atlanta, GA, USA. ⁹¹Department of Internal Medicine, Seoul National University Hospital, Seoul, South Korea. ⁹²Institute of Clinical Medicine, The University of Eastern Finland, Kuopio, Finland. ⁹³Kuopio University Hospital, Kuopio, Finland. ⁹⁴Department of Clinical Chemistry, Fimlab Laboratories and Finnish Cardiovascular Research Center-Tampere, Faculty of Medicine and Health Technology, Tampere University, Tampere, Finland. ⁹⁵The Mindich Child Health and Development Institute, Icahn School of Medicine at Mount Sinai, New York, NY, USA. ⁹⁶Li Ka Shing Institute of Health Sciences, The Chinese University of Hong Kong, Hong Kong, China. ⁹⁷Hong Kong Institute of Diabetes and Obesity, The Chinese University of Hong Kong, Hong Kong, China. ⁹⁸Cardiovascular Research REGICOR Group, Hospital del Mar Medical Research Institute (IMIM), Barcelona, Catalonia, Spain. ⁹⁹Department of Genetics, Harvard Medical School, Boston, MA, USA. ¹⁰⁰Oxford Centre for Diabetes, Endocrinology and Metabolism, University of Oxford, Churchill Hospital, Headington, Oxford, UK. ¹⁰¹Wellcome Centre for Human Genetics, University of Oxford, Oxford, UK. ¹⁰²Oxford NIHR Biomedical Research Centre, Oxford University Hospitals NHS Foundation Trust, John Radcliffe Hospital, Oxford, UK. ¹⁰³F Widjaja Foundation Inflammatory Bowel and Immunobiology Research Institute, Cedars-Sinai Medical Center, Los Angeles, CA, USA. ¹⁰⁴Atherogenomics Laboratory, University of Ottawa Heart Institute, Ottawa, Canada. ¹⁰⁵Division of General Internal Medicine, Massachusetts General Hospital, Boston, MA, USA. ¹⁰⁶Department of Clinical Sciences, University Hospital Malmö Clinical Research Center, Lund University, Malmö, Sweden. ¹⁰⁷Department of Clinical Sciences, Lund University, Skane University Hospital, Malmö, Sweden. ¹⁰⁸Instituto Nacional de Medicina Genómica (INMEGEN), Mexico City, Mexico. ¹⁰⁹Medical Research Institute, Ninewells Hospital and Medical School, University of Dundee, Dundee, UK. ¹¹⁰Department of Molecular Medicine and Biopharmaceutical Sciences, Graduate School of Convergence Science and Technology, Seoul National University, Seoul, South Korea. ¹¹¹Department of Psychiatry, Keck School of Medicine at the University of Southern California, Los Angeles, CA, USA. ¹¹²Department of Psychiatry and Behavioral Sciences, Johns Hopkins University School of Medicine, Baltimore, MD, USA. ¹¹³Division of Genetics and Epidemiology, Institute of Cancer Research, London, UK. ¹¹⁴Medical Research Center, Oulu University Hospital, Oulu, Finland and Research Unit of Clinical Neuroscience, Neurology, University of Oulu, Oulu, Finland. ¹¹⁵Research Center, Montreal Heart Institute, Montreal, Quebec, Canada. ¹¹⁶Department of Medicine, Faculty of Medicine, Université de Montréal, Quebec, Canada. ¹¹⁷Department of Biomedical Informatics, Vanderbilt University Medical Center, Nashville, TN, USA. ¹¹⁸Department of Medicine, Vanderbilt University Medical Center, Nashville, TN, USA. ¹¹⁹Department of Biostatistics and

Epidemiology, Perelman School of Medicine at the University of Pennsylvania, Philadelphia, PA, USA. ¹²⁰Department of Medicine, Perelman School of Medicine at the University of Pennsylvania, Philadelphia, PA, USA. ¹²¹Center for Non-Communicable Diseases, Karachi, Pakistan. ¹²²National Institute for Health and Welfare, Helsinki, Finland. ¹²³Deutsches Herzzentrum München, Munich, Germany. ¹²⁴Technische Universität München, Munich, Germany. ¹²⁵Division of Cardiovascular Medicine, Nashville VA Medical Center and Vanderbilt University, School of Medicine, Nashville, TN, USA. ¹²⁶Department of Psychiatry, Icahn School of Medicine at Mount Sinai, New York, NY, USA. ¹²⁷Department of Genetics and Genomic Sciences, Icahn School of Medicine at Mount Sinai, New York, NY, USA. ¹²⁸Institute for Genomics and Multiscale Biology, Icahn School of Medicine at Mount Sinai, New York, NY, USA. ¹²⁹Institute of Clinical Medicine, Neurology, University of Eastern Finland, Kuopio, Finland. ¹³⁰Department of Twin Research and Genetic Epidemiology, King's College London, London, UK. ¹³¹Departments of Genetics and Psychiatry, University of North Carolina, Chapel Hill, NC, USA. ¹³²Saw Swee Hock School of Public Health, National University of Singapore, National University Health System, Singapore, Singapore. ¹³³Department of Medicine, Yong Loo Lin School of Medicine, National University of Singapore, Singapore, Singapore. ¹³⁴Duke-NUS Graduate Medical School, Singapore, Singapore. ¹³⁵Life Sciences Institute, National University of Singapore, Singapore, Singapore. ¹³⁶Department of Statistics and Applied Probability, National University of Singapore, Singapore, Singapore. ¹³⁷Folkhälsan Institute of Genetics, Folkhälsan Research Center, Helsinki, Finland. ¹³⁸HUCH Abdominal Center, Helsinki University Hospital, Helsinki, Finland. ¹³⁹Center for Behavioral Genomics, Department of Psychiatry, University of California, San Diego, CA, USA. ¹⁴⁰Institute of Genomic Medicine, University of California, San Diego, CA, USA. ¹⁴¹Juliet Keidan Institute of Pediatric Gastroenterology, Shaare Zedek Medical Center, The Hebrew University of Jerusalem, Jerusalem, Israel. ¹⁴²Instituto de Investigaciones Biomédicas UNAM, Mexico City, Mexico. ¹⁴³Instituto Nacional de Ciencias Médicas y Nutrición Salvador Zubirán, Mexico City, Mexico. ¹⁴⁴Radcliffe Department of Medicine, University of Oxford, Oxford, UK. ¹⁴⁵Department of Gastroenterology and Hepatology, University of Groningen and University Medical Center Groningen, Groningen, The Netherlands. ¹⁴⁶Department of Physiology and Biophysics, University of Mississippi Medical Center, Jackson, MS, USA. ¹⁴⁷Program in Infectious Disease and Microbiome, Broad Institute of MIT and Harvard, Cambridge, MA, USA. ¹⁴⁸Center for Computational and Integrative Biology, Massachusetts General Hospital, Boston, MA, USA. ¹⁵¹Deceased: Pamela Sklar.

Reporting summary

Further information on research design is available in the Nature Research Reporting Summary linked to this paper.

Data availability

The gnomAD 2.1.1 dataset is available for download at <http://gnomad.broadinstitute.org>, where we have developed a browser for the dataset and provide files with detailed frequency and annotation information for each variant. There are no restrictions on the aggregate data released.

Code availability

All code to perform quality control is provided at https://github.com/broadinstitute/gnomad_qc, and the code to perform all analyses and regenerate all the figures in this manuscript is provided at https://github.com/macarthur-lab/gnomad_lof. LOFTEE is available at <https://github.com/konradjk/loftee>. All code and software to reproduce figures are available in a Docker image at [konradjk/gnomad_lof_paper:0.2](https://github.com/konradjk/gnomad_lof_paper).

Acknowledgements We thank the many individuals whose sequence data are aggregated in gnomAD for their contributions to research, and the users of gnomAD for their collaborative feedback. We also thank D. Altshuler for contributions to the development of the gnomAD resource, and A. Martin, E. Fauman, J. Bloom, D. King and the Hail team for discussions. The results published here are in part based on data: (1) generated by The Cancer Genome Atlas (TCGA) managed by the NCI and NHGRI (accession: phs000178.v10.p8); information about TCGA can be found at <http://cancergenome.nih.gov>; (2) generated by the Genotype-Tissue Expression Project (GTEx) managed by the NIH Common Fund and NHGRI (accession: phs000424.v7.p2); (3) generated by the Exome Sequencing Project, managed by NHLBI; (4) generated by the Alzheimer's Disease Sequencing Project (ADSP), managed by the NIA and NHGRI (accession: phs000572.v7.p4). K.J.K. was supported by NIGMS F32 GM115208. L.C.F. was supported by the Swiss National Science Foundation (Advanced Postdoc.Mobility 177853). J.X.C. was supported by NHGRI and NHLBI grants UM1 HG006493 and U24 HG008956. Analysis of the Genome Aggregation Database was funded by NIDDK U54 DK105566, NHGRI UM1 HG008900, BioMarin Pharmaceutical Inc., and Sanofi Genzyme Inc.

Development of LOFTEE was funded by NIGMS R01 GM104371. D.G.M., R.L.C., and M.E.T. were supported by NICHHD HD081256. D.G.M., R.L.C. and M.E.T. were supported by NIMH MH115957. The complete acknowledgments can be found in the Supplementary Information. We have complied with all relevant ethical regulations.

Author contributions K.J.K., L.C.F., G.T., B.B.C., J.A., Q.W., R.L.C., K.M.L., A.G., M.S., D.R., M.S.-B., B.M.N., M.J.D. and D.G.M. contributed to the writing of the manuscript and generation of figures. K.J.K., L.C.F., G.T., B.B.C., Q.W., R.L.C., K.M.L., A.G., H.B., D.R., M.S.-B., E.M.E., E.G.S., J.A.K., N.W., J.X.C., K.E.S., E.P.-H., Z.Z., A.H.O'D.-L., M.E.T., B.M.N., M.J.D. and D.G.M. contributed to the analysis of data. K.J.K., L.C.F., G.T., B.B.C., K.M.L., D.P.B., L.D.G., M.S., N.A.W., R.K.W., K.T., Y.F., E.B., T.P., A.W., C.S., K.E.S., Z.Z., A.H.O'D.-L., C.V., B.M.N., M.J.D. and D.G.M. developed tools and methods that enabled the scientific discoveries herein. K.J.K., L.C.F., G.T., B.B.C., J.A., R.L.C., K.M.L., L.D.G., Y.F., E.B., A.H.O'D.-L., E.V.M., B.W., M.L., J.S.W., C.V., I.M.A., L.B., K.C., K.M.C., M.C., S.D., S.F., S.G., J.G., N.G., T.J., D.K., C.L., R.M., S.N., N.P., D.R., V.R.-R., A.S., M.S., J.S., K.T., C.T., G.W., M.E.T., B.M.N., M.J.D. and D.G.M. contributed to the production and quality control of the gnomAD dataset. All authors listed under The Genome Aggregation Database Consortium contributed to the generation of the primary data incorporated into the gnomAD resource. All authors reviewed the manuscript.

Competing interests K.J.K. owns stock in Personalis. R.K.W. has received unrestricted research grants from Takeda Pharmaceutical Company. A.H.O'D.-L. has received honoraria from ARUP and Chan Zuckerberg Initiative. E.V.M. has received research support in the form of charitable contributions from Charles River Laboratories and Ionis Pharmaceuticals, and has consulted for Deerfield Management. J.S.W. is a consultant for MyoKardia. B.M.N. is a member of the scientific advisory board at Deep Genomics and consultant for Camp4 Therapeutics, Takeda Pharmaceutical, and Biogen. M.J.D. is a founder of Maze Therapeutics. D.G.M. is a founder with equity in Goldfinch Bio, and has received research support from AbbVie, Astellas, Biogen, BioMarin, Eisai, Merck, Pfizer, and Sanofi-Genzyme. The views expressed in this article are those of the author(s) and not necessarily those of the NHS, the NIHR, or the Department of Health. M.I.M. has served on advisory panels for Pfizer, NovoNordisk, Zoe Global; has received honoraria from Merck, Pfizer, NovoNordisk and Eli Lilly; has stock options in Zoe Global and has received research funding from Abbvie, Astra Zeneca, Boehringer Ingelheim, Eli Lilly, Janssen, Merck, NovoNordisk, Pfizer, Roche, Sanofi Aventis, Servier & Takeda. As of June 2019, M.I.M. is an employee of Genentech, and holds stock in Roche. N.R. is a non-executive director of AstraZeneca.

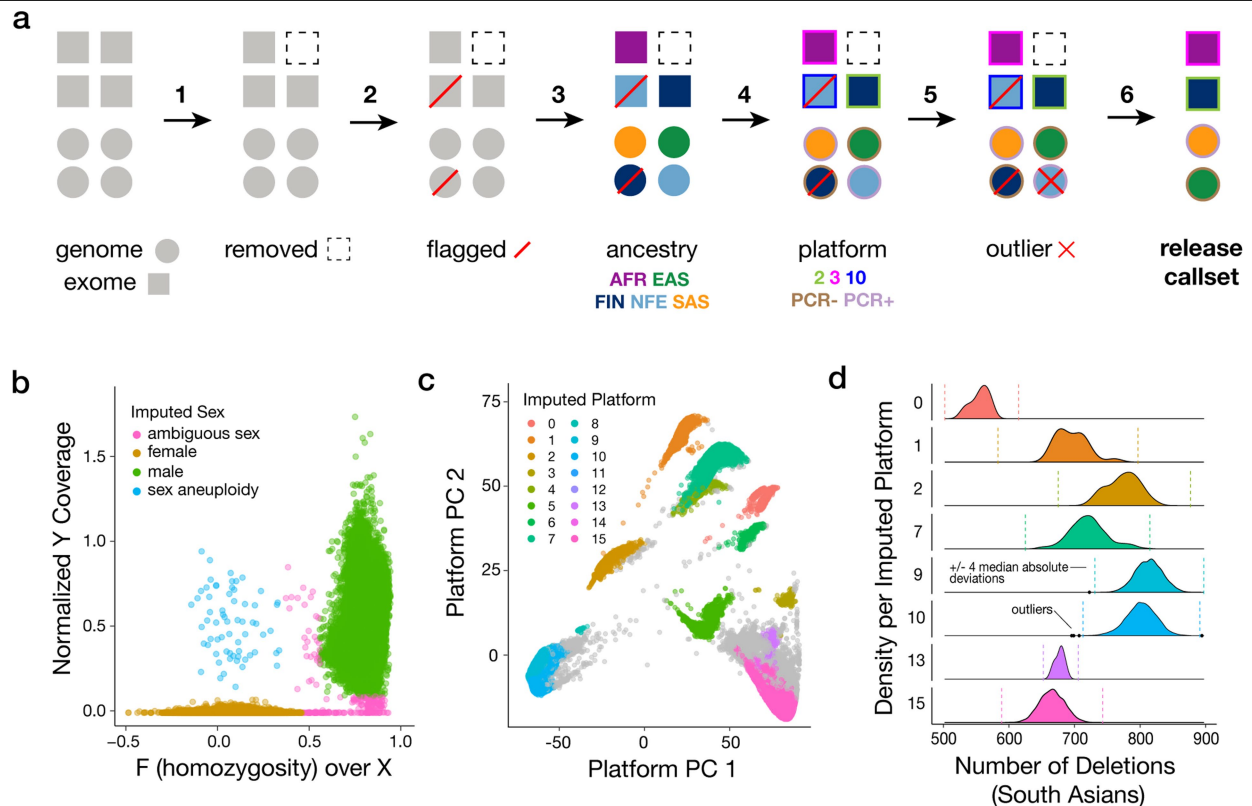
Additional information

Supplementary information is available for this paper at <https://doi.org/10.1038/s41586-020-2308-7>.

Correspondence and requests for materials should be addressed to K.J.K. or D.G.M.

Peer review information Nature thanks Deanna Church, Rayna Harris, Alexander Hoischen and the other, anonymous, reviewers for their contribution to the peer review of this work. Peer reviewer reports are available.

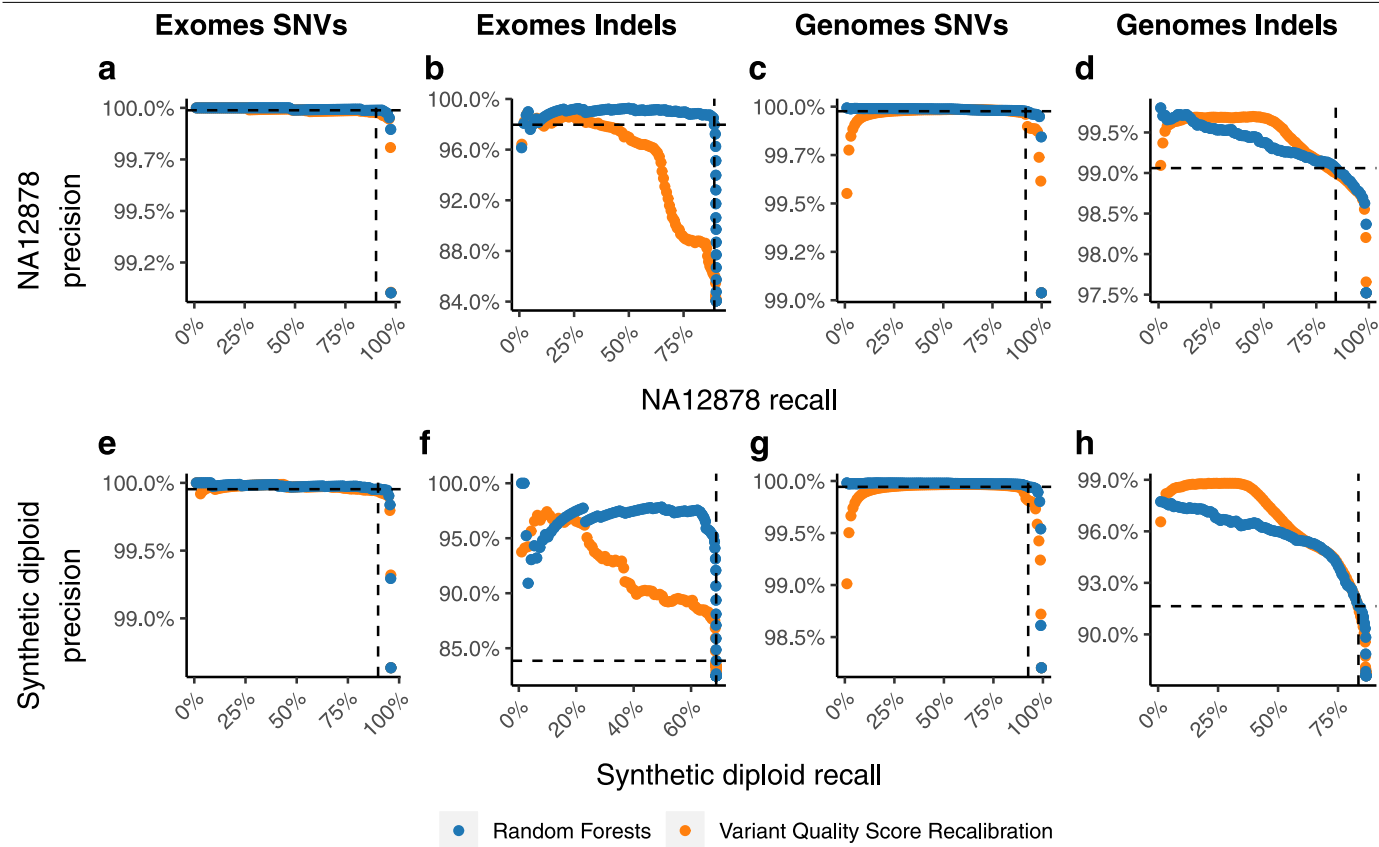
Reprints and permissions information is available at <http://www.nature.com/reprints>.



Extended Data Fig. 1 | Overview of the sample quality control workflow.

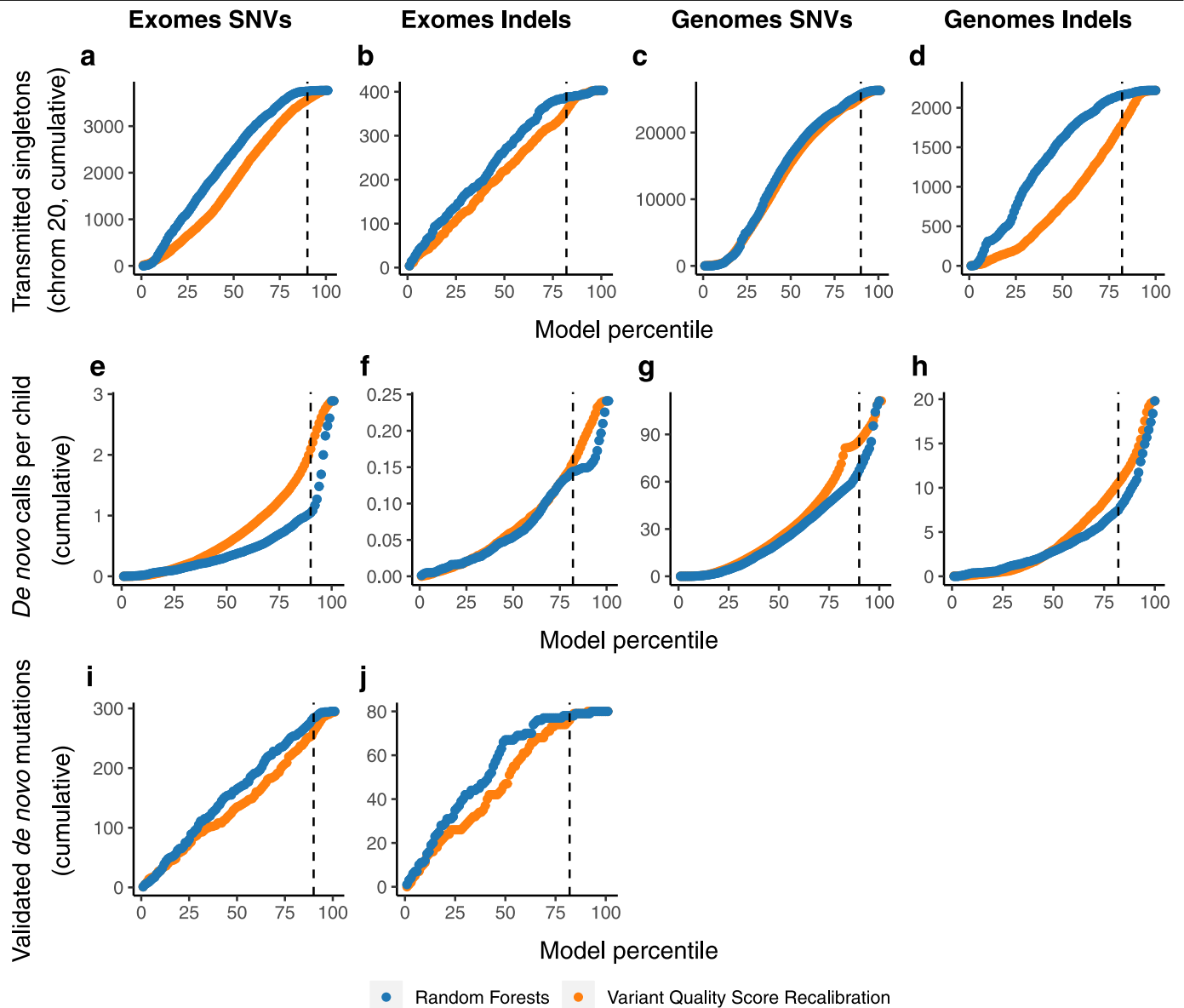
a. Exome (square) and genome (circle) samples underwent quality control in the following stages: hard filtering (step 1), relatedness inference (step 2), ancestry inference (step 3), platform inference (step 4, for exomes only), and population- and platform-specific outlier filtering (step 5). See Supplementary Information for further details. Except for samples failing hard filters (dotted outline), all quality control analyses were applied to all samples, regardless of the presence or absence of other quality control flags (such as relatedness, lack of release permissions, or outlier status; red diagonal bar). Assignment of ancestry labels is represented by fill colour and accompanying three-letter ancestry group abbreviation. Assignment of platform labels is represented by outline colour and a numbered label for exomes (corresponding to imputed platforms) and a PCR \pm label for genomes. The final set of samples included in the gnomAD release (125,748 exomes and 15,708 genomes) was defined to be the set of unrelated samples with release permissions, no hard filter flags, and no population- and platform-specific outlier metrics (step 6). **b.** In exomes, the

chromosomal sex of samples was inferred based on the inbreeding coefficient on chromosome X and the coverage of chromosome Y into male (green), female (amber), ambiguous sex (pink), and sex chromosome aneuploid (blue). **c.** The top two principal components from PCA-HDBSCAN analysis of exome capture regions. Sequencing platforms were inferred for exome samples based on principal component analysis of biallelic variant call rates over all known exome capture regions, and samples were assigned a cluster label (0–15, or unknown) using HDBSCAN. **d.** We performed platform- and population-specific outlier filtering for several quality-control metrics. The distribution of the number of deletions in samples from south Asian individuals across platforms is shown. Distributions (and accordingly, median and median absolute deviations) for these metrics varied widely both by population and sequencing platform (numbered on the y axis). Outliers (black dots) were defined as samples with values outside four median absolute deviations (shown by dotted vertical lines) from the median of a given metric.



Extended Data Fig. 2 | Variant calling performance for common variants. **a–h**, Precision-recall curves are shown for variant calls in two samples with independent gold-standard data, NA12878⁴⁹ (**a–d**) and a synthetic diploid mixture⁵⁰ (**e–h**). The random forest (blue) approach described here is compared to the current state-of-the-art GATK variant quality score recalibration (orange) for exome SNVs (**a, e**) and indels (**b, f**), and genome SNVs

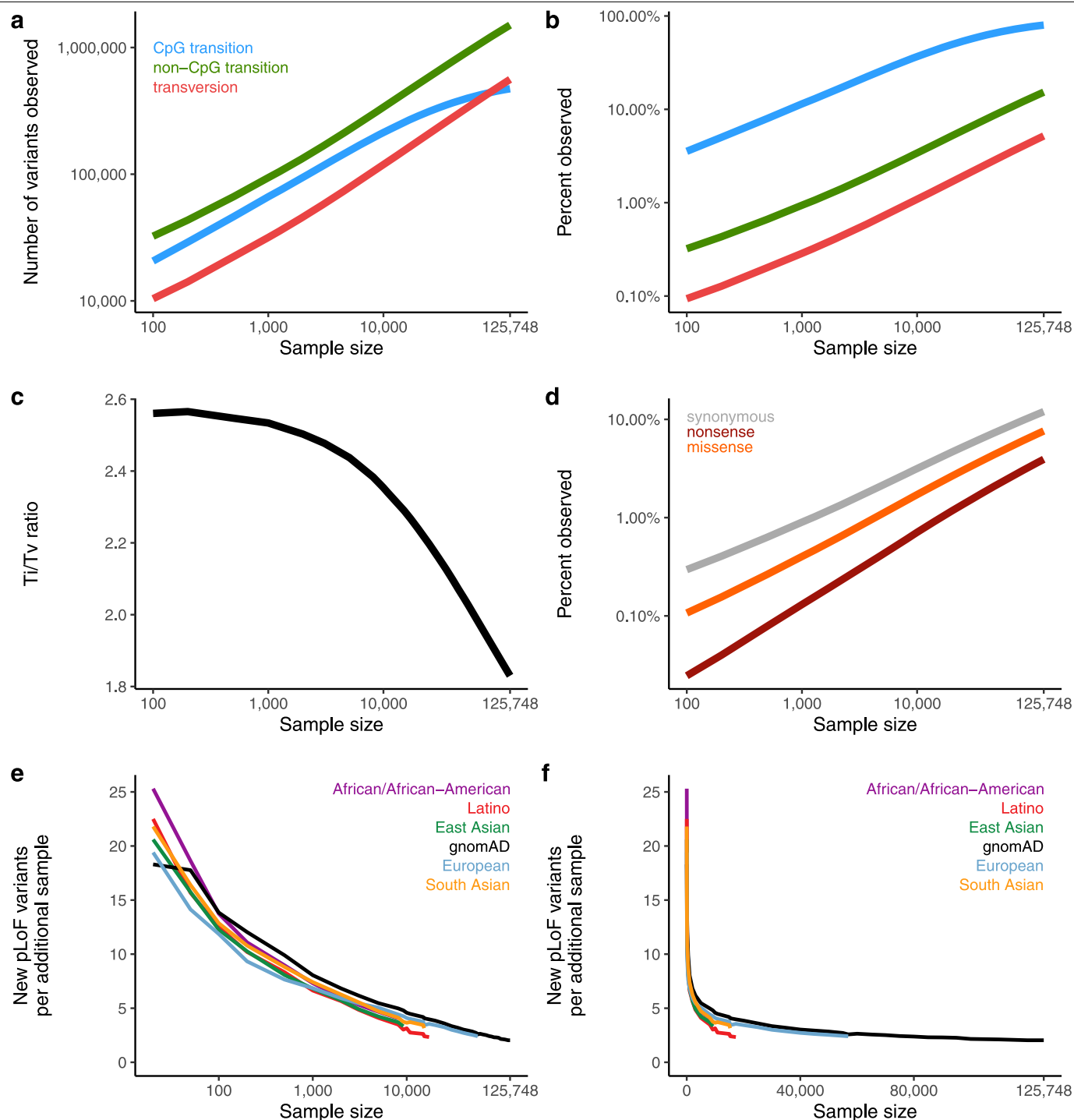
(**c, g**) and indels (**d, h**). Note that the indels presented in **f** and **h** exclude 1-base-pair (bp) indels as they are not well characterized in the synthetic diploid mixture gold standard sample. In all cases, at the thresholds chosen (dashed lines representing 10% and 20% of SNVs and indels filtered, respectively), random forest outperforms or is similar to variant quality score recalibration.



Extended Data Fig. 3 | Variant calling performance for rare variants.

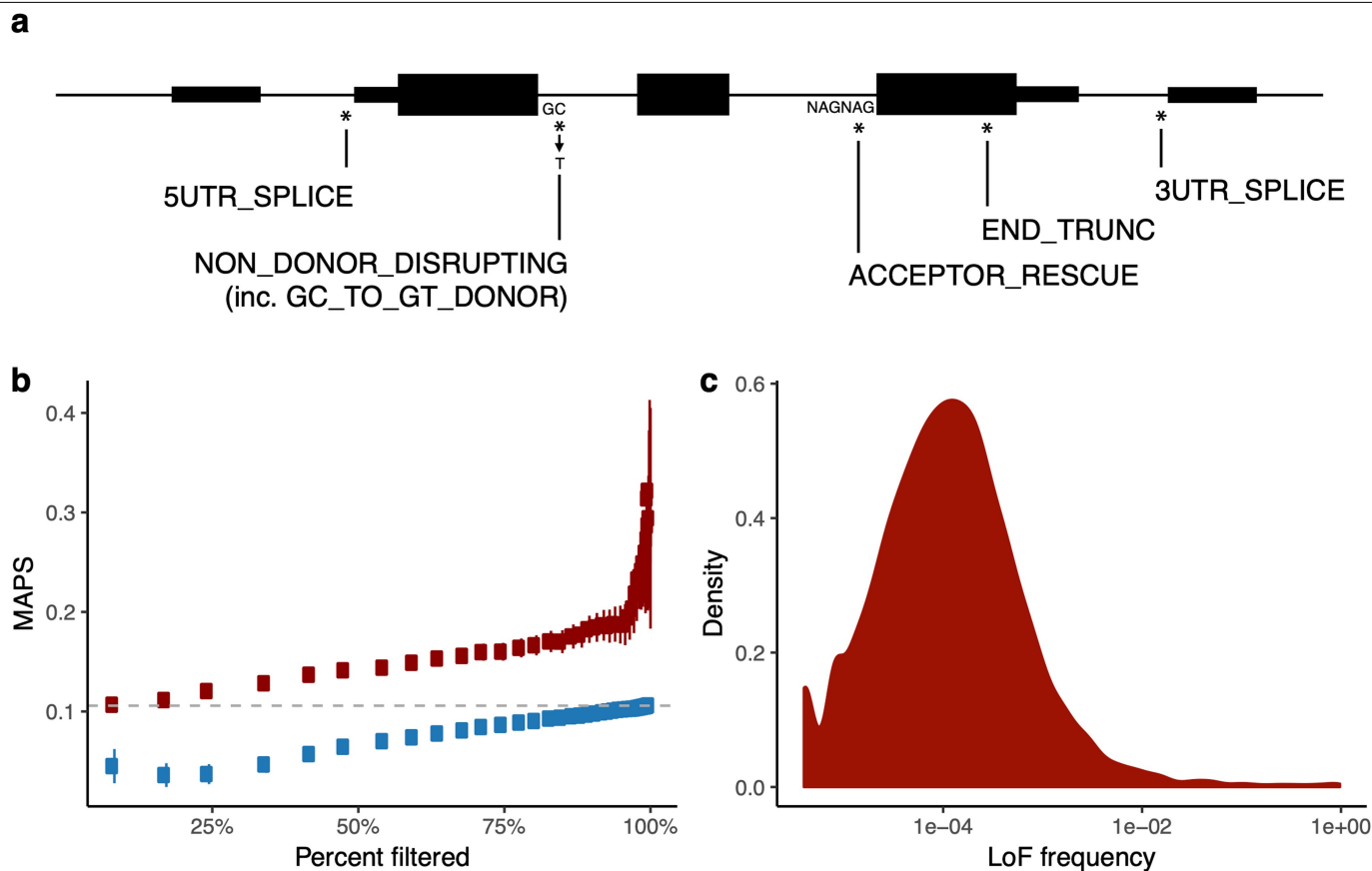
a–j. The x axes show the cumulative ranked percentile for our random forest (blue) model and, as a comparison, for the current state-of-the-art GATK variant quality score recalibration (orange). That is, the point at 10 shows the performance of the 10% best-scored data; the point at 50 shows the performance 50% best-scored data. **a–d.** The number of transmitted singletons (singletons in the unrelated individuals that are transmitted to an offspring) on chromosome 20 for exome SNVs (**a**) and indels (**b**), and genome SNVs (**c**) and indels (**d**). Chromosome 20 was not used for training our random forest model. We expect most of these to be real variants because we observe Mendelian

transmission of an allele that was sequenced independently in a parent and child. **e–h.** The number of bi-allelic de novo calls per child (4,568 exomes, 212 genomes) outside of low-complexity regions. The expectation is that there is approximately 1.6 de novo SNV (**e**) and 0.1 de novo indels per exome (**f**), and 65 de novo SNVs (**g**) and 5 de novo indels (**h**) per genome²⁰. **i, j.** The number of independently validated de novo mutations, available for a subset of 331 exome samples for which de novo mutations were validated as part of other studies⁵¹. In all cases, at the thresholds chosen (dashed lines representing 10% and 20% of SNVs and indels filtered, respectively), random forest outperforms or is similar to variant quality score recalibration.



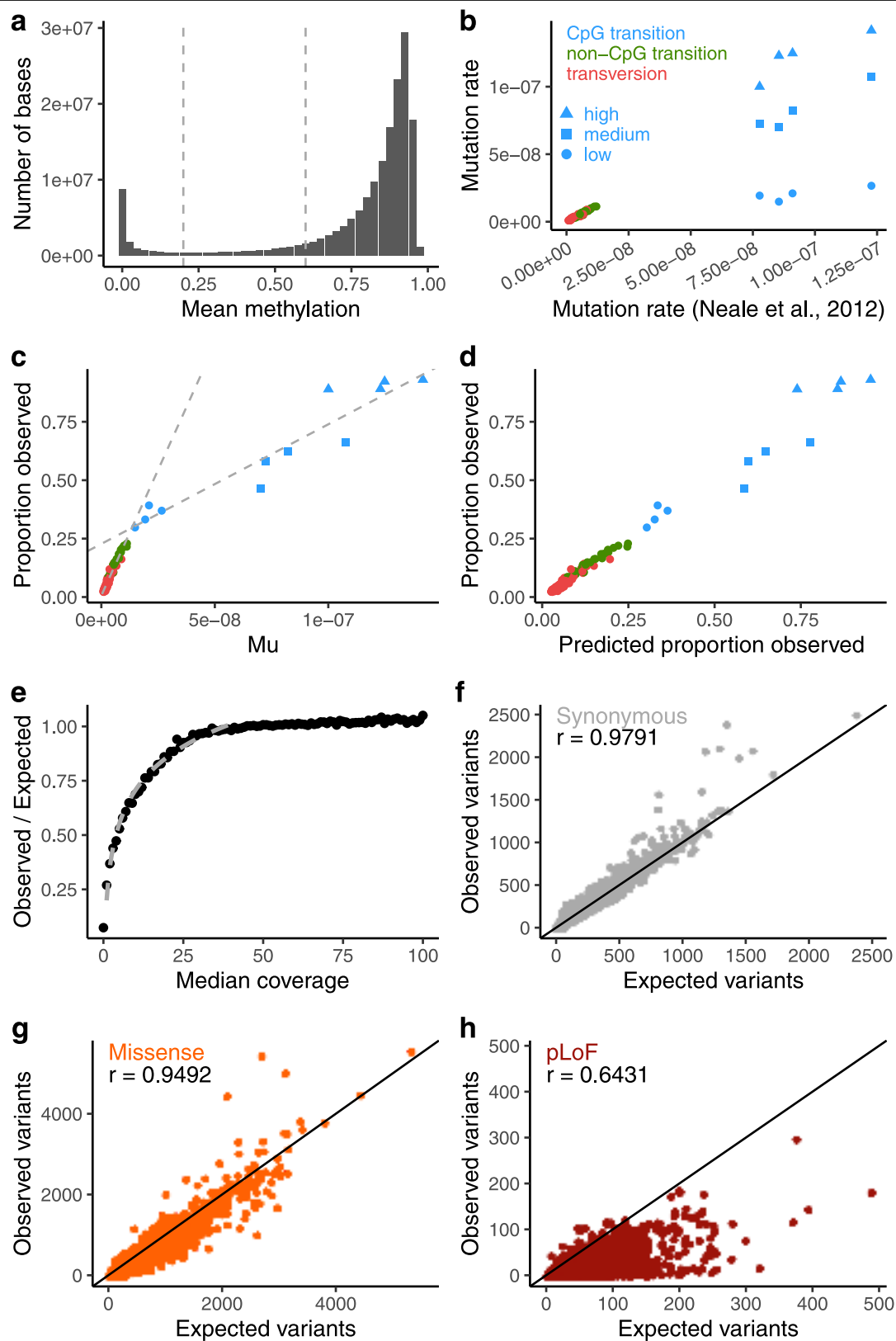
Extended Data Fig. 4 | Variant discovery at large sample sizes. **a, b**, The total number of variants observed (**a**) and the proportion of possible variants observed (**b**) as a function of sample size, broken down by variant class. At large sample sizes, CpG transitions become saturated, as previously described⁴. Colours are consistent in **a** and **b**. **c**, This results in a decrease of the transition/transversion (Ti/Tv) ratio. **d**, When broken down by functional class, we

observe the effects of selection, in which synonymous variants have the highest proportion observed, followed by missense and pLoF variants. **e, f**, The number of additional pLoF variants introduced into the cohort as a function of sample size on a log (**e**) and linear (**f**) scale. Here, gnomAD (black) refers to a uniform sampling from the population distribution of the full cohort of exome-sequenced individuals.



Extended Data Fig. 5 | Using LofTEE to create a high-confidence set of pLoF variation. **a**, Schematic of LofTEE filters. LofTEE filters out putative stop-gained, essential splice, and frameshift variants based on sequence and transcript context, as well as flagging exonic features such as conservation (not shown). For instance, variants that are not predicted to disrupt splicing based on retention of a strong splice site, or rescue of a nearby splice site. Additional filters not shown include: ANC_ALLELE (the alternative allele is the ancestral allele), NON_ACCEPTOR_DISRUPTING and DONOR_RESCUE (opposite to those already shown). **b**, To tune the END_TRUNC filter, we retained variants that pass the 50-bp rule (are more than 50 bp before the 3'-most splice site). The overall

MAPS score for variants that fail this rule is shown in grey. For the remaining 39,072 variants, we computed the sum of the genomic evolutionary rate profiling (GERP) score of bases deleted by the variant. At 40 bins of this score, we compute the MAPS score for those variants retained at this threshold (red) compared to variants removed at this threshold (blue), and plot this as a function of the proportion of variants filtered at this threshold. We chose the 50% point as it retains variants with a MAPS score of 0.14, while removing variants with a MAPS score of 0.06. Error bars represent 95% confidence intervals. **c**, Density plot of aggregate pLoF frequency computed from high-confidence pLoF variants discovered using LofTEE.

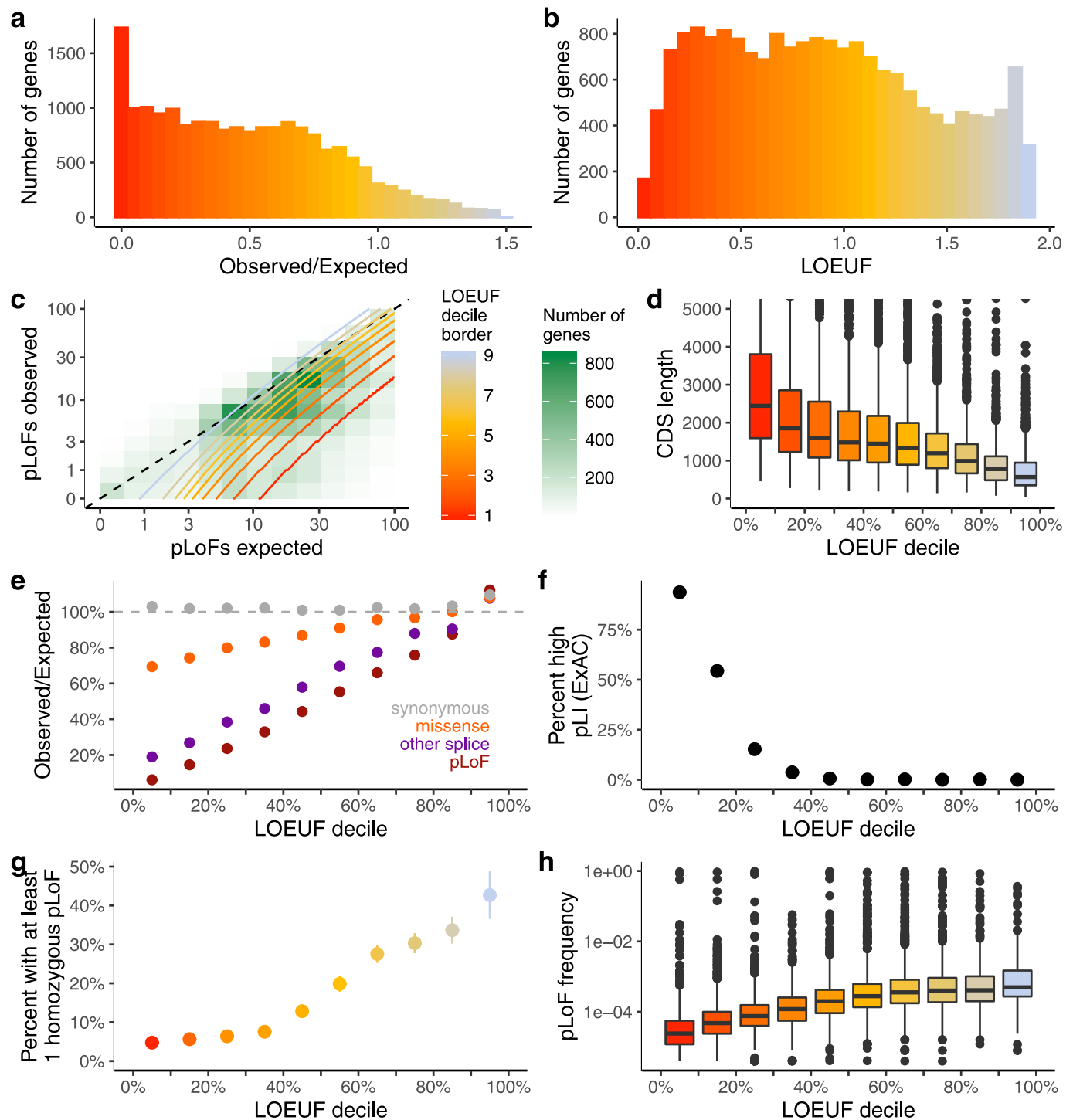


Extended Data Fig. 6 | See next page for caption.

Extended Data Fig. 6 | Computing the depletion of variation of functional categories. **a**, The distribution of mean methylation values across 37 tissues and across every CpG dinucleotide in the genome. We divided the genome into 3 levels (low methylation, missing or < 0.2 ; medium, $0.2 - 0.6$; and high, > 0.6) and computed all ensuing metrics based on these categories. **b**, Comparison of estimates of the mutation rate with previous estimates⁵². For transversions and non-CpG transitions, we observe a strong correlation (linear regression $r = 0.98$; $P = 2.6 \times 10^{-65}$). For CpG transitions, the new estimates are calculated separately for the three levels of methylation and track with these levels. Colours and shapes are consistent in **b-d**. **c**, For **c-e**, only synonymous variants are considered. The proportion of possible variants observed for each context is correlated with the mutation rate. We compute two fit lines, one for CpG

transitions, and one for other contexts to calibrate our estimates.

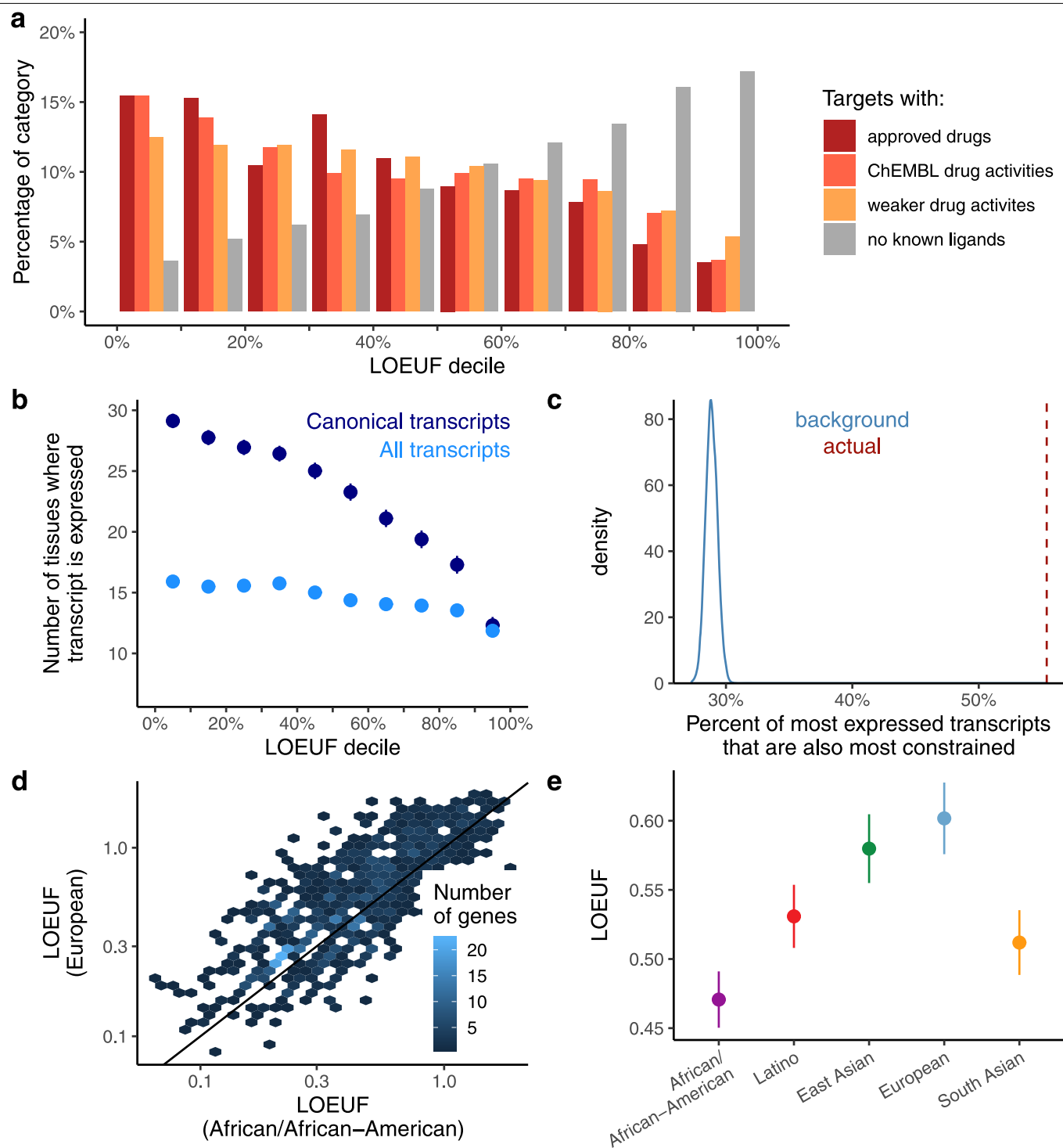
d, Calibration of each context to compute a predicted proportion observed after fitting the two models in **c**, which is used to calculate an expected number of variants at high coverage. **e**, With an expectation computed from high coverage regions, the observed/expected ratio follows a logarithmic trend with the median coverage below $40\times$, which is used to correct low coverage bases in the final expectation model. **f-h**, For each transcript, the observed number of variants is plotted against the expected number from the model described above, for synonymous (**f**), missense (**g**), and pLoF (**h**) variants, and the linear regression coefficient is shown. Note that the expectation does not include selection, and so, pLoF and, to a lesser extent, missense variants exhibit lower observed values than expected.



Extended Data Fig. 7 | Genomic properties of constrained genes.

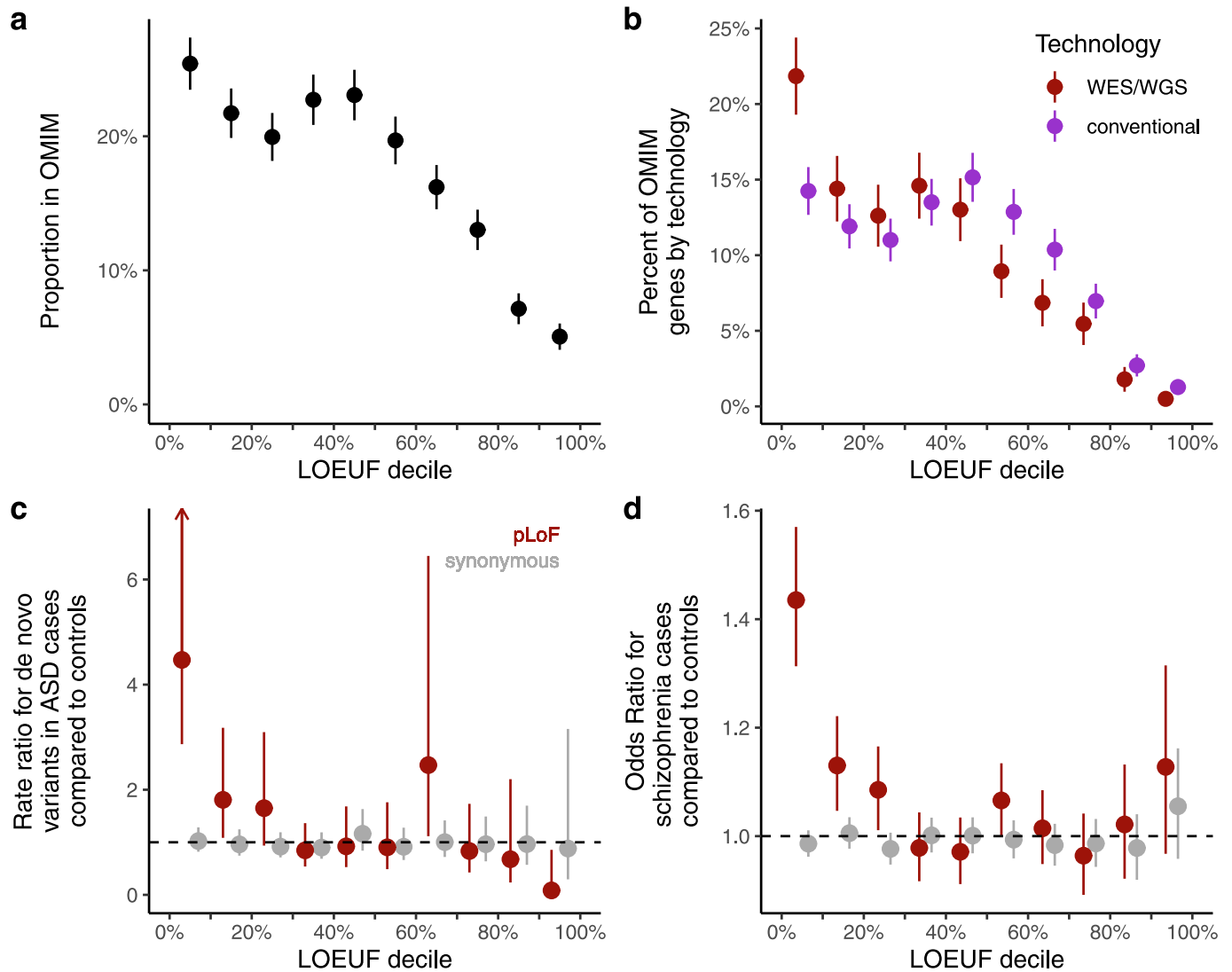
a, b, Histogram of the observed/expected ratio of pLoF variation (**a**) and LOEUF (**b**). Most genes have fewer observed variants than expected (median observed/expected = 0.48), and the genes with no observed pLoFs are distinguished between confidently constrained genes and noise by LOEUF. **c**, A 2D density plot of the number of observed versus expected pLoF variants. The boundaries of each decile are plotted as gradients (that is, the most constrained decile is below the lowest red line). **d**, The LOEUF of a gene is correlated with its coding sequence length ($\beta = -1.07 \times 10^{-4}$; $P < 10^{-100}$); thus, for all downstream statistical tests, we adjust for gene length or remove genes with fewer than 10 expected pLoFs. **e**, Observed/expected ratios of various functional classes

across genes within each LOEUF decile. The most constrained decile has approximately 6% of the expected pLoFs, while synonymous variants are not depleted and missense variants exhibit modest depletion. **f**, The percentage of each LOEUF decile that was described in ExAC as constrained, or $pLI > 0.9^4$. **g**, The percentage of each LOEUF decile that have at least one homozygous pLoF variant. **h**, Box plots of the aggregate pLoF frequency for each LOEUF decile. Centre line denotes the median; box limits denote upper and lower quartiles; whiskers denote $1.5 \times$ the interquartile range; points denote outliers. In **e–g**, error bars represent 95% confidence intervals (note that in some cases these are fully contained within the plotted point).



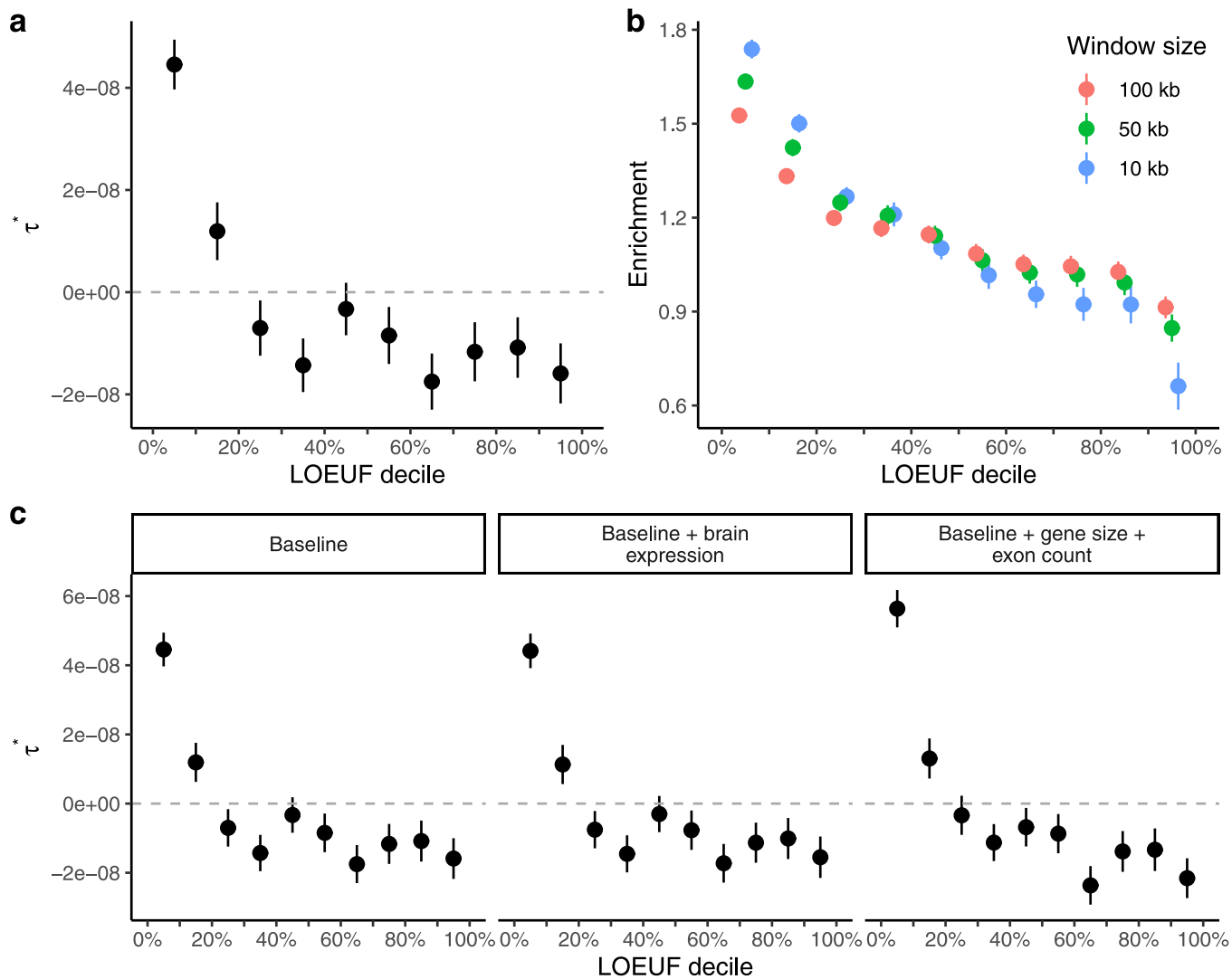
Extended Data Fig. 8 | Biological properties of constrained genes. a, The percentage of genes in each functional category from Pharos (see Supplementary Information) is broken down by the LOEUF decile. **b,** The mean number of tissues in which a transcript is expressed, binned by transcript-based LOEUF decile, is shown for all transcripts and canonical transcripts. **c,** The percentage of genes in which the most expressed transcript is also the most constrained is plotted in red, which is enriched compared to a permuted set (blue). **d,** For 927 genes with expected pLoF ≥ 10 in both the

African/African American and European population subsets ($n = 8,128$), the LOEUF scores are highly correlated (linear regression $r = 0.78$, $P < 10^{-100}$), with a lower mean score observed in the African/African American population (0.49 versus 0.62; two-sided t -test $P = 4.1 \times 10^{-14}$), which has a higher effective population size. **e,** The mean LOEUF score for 865 genes with expected pLoF ≥ 10 in all populations ($n = 8,128$). Error bars represent 95% confidence intervals.



Extended Data Fig. 9 | Applications of constraint metrics to rare variant analysis of disease. **a**, Proportion of each LOEUF decile found in OMIM. **b**, Proportion of disease-associated genes discovered by whole-exome/genome sequencing (WES/WGS) compared to conventional (typically linkage) methods, plotted by LOEUF decile. The former are more constrained (LOEUF 0.674 versus 0.806, two-sided t -test $P = 1.2 \times 10^{-16}$), which suggests that these techniques are more effective for picking up genes with a de novo

mechanism of disease, compared to recessive genes identified by linkage methods. **c**, Similar to Fig. 5a, the rate ratio is defined by the rate of de novo variants (number per patient) in autism cases divided by the rate in controls. pLoF variants in the most constrained decile of the genome are approximately fourfold more likely to be found in cases compared to controls. **d**, The mean odds ratio of a logistic regression of schizophrenia²⁸ is plotted for each LOEUF decile. Error bars in **a–d** correspond to 95% confidence intervals.



Extended Data Fig. 10 | Applications of constraint metrics to common variant analysis of disease. a. The τ^* coefficient (see Supplementary Information) for each LOEUF decile across 276 independent traits. Unlike the enrichment measure reported in Fig. 5, τ^* is adjusted for 74 baseline genomics annotations. Positive values of τ^* indicate greater per-SNP heritability than would be expected based on the other annotations in the baseline model, whereas negative values indicate depleted per-SNP heritability compared to

that baseline expectation. **b.** Enrichment coefficient for each LOEUF decile using different window sizes to define which SNPs to include upstream and downstream of each gene. **c.** Enrichment coefficient for each LOEUF decile across traits after controlling for brain expression and gene size. Results are consistent with those shown in Fig. 5, which indicates that brain gene expression and gene size do not fully explain the enrichment of heritability observed in constrained genes. Error bars represent 95% confidence intervals.

Reporting Summary

Nature Research wishes to improve the reproducibility of the work that we publish. This form provides structure for consistency and transparency in reporting. For further information on Nature Research policies, see [Authors & Referees](#) and the [Editorial Policy Checklist](#).

Statistics

For all statistical analyses, confirm that the following items are present in the figure legend, table legend, main text, or Methods section.

- | | |
|-------------------------------------|--|
| n/a | Confirmed |
| <input type="checkbox"/> | <input checked="" type="checkbox"/> The exact sample size (n) for each experimental group/condition, given as a discrete number and unit of measurement |
| <input type="checkbox"/> | <input checked="" type="checkbox"/> A statement on whether measurements were taken from distinct samples or whether the same sample was measured repeatedly |
| <input type="checkbox"/> | <input checked="" type="checkbox"/> The statistical test(s) used AND whether they are one- or two-sided
<i>Only common tests should be described solely by name; describe more complex techniques in the Methods section.</i> |
| <input type="checkbox"/> | <input checked="" type="checkbox"/> A description of all covariates tested |
| <input type="checkbox"/> | <input checked="" type="checkbox"/> A description of any assumptions or corrections, such as tests of normality and adjustment for multiple comparisons |
| <input type="checkbox"/> | <input checked="" type="checkbox"/> A full description of the statistical parameters including central tendency (e.g. means) or other basic estimates (e.g. regression coefficient) AND variation (e.g. standard deviation) or associated estimates of uncertainty (e.g. confidence intervals) |
| <input type="checkbox"/> | <input checked="" type="checkbox"/> For null hypothesis testing, the test statistic (e.g. F , t , r) with confidence intervals, effect sizes, degrees of freedom and P value noted
<i>Give P values as exact values whenever suitable.</i> |
| <input checked="" type="checkbox"/> | <input type="checkbox"/> For Bayesian analysis, information on the choice of priors and Markov chain Monte Carlo settings |
| <input checked="" type="checkbox"/> | <input type="checkbox"/> For hierarchical and complex designs, identification of the appropriate level for tests and full reporting of outcomes |
| <input type="checkbox"/> | <input checked="" type="checkbox"/> Estimates of effect sizes (e.g. Cohen's d , Pearson's r), indicating how they were calculated |

Our web collection on [statistics for biologists](#) contains articles on many of the points above.

Software and code

Policy information about [availability of computer code](#)

Data collection No software was used for the collection of data, as this was an opportunistic study.

Data analysis All code to perform quality control and data analysis is provided in the following Github repos:

https://github.com/macarthur-lab/gnomad_qc
https://github.com/macarthur-lab/gnomad_lof
<https://github.com/konradjk/loftee>

Hail 0.2 is available at: <https://hail.is/>

Picard version 1.1431

VerifyBamID version 1.0.0

GATK nightly-2015-07-31-g3c929b0, 3.4-89-ge494930, and 3.6-0-g89b7209

For manuscripts utilizing custom algorithms or software that are central to the research but not yet described in published literature, software must be made available to editors/reviewers. We strongly encourage code deposition in a community repository (e.g. GitHub). See the Nature Research [guidelines for submitting code & software](#) for further information.

Data

Policy information about [availability of data](#)

All manuscripts must include a [data availability statement](#). This statement should provide the following information, where applicable:

- Accession codes, unique identifiers, or web links for publicly available datasets
- A list of figures that have associated raw data
- A description of any restrictions on data availability

All datasets are described in the manuscript or Supplementary Information, including deposition of the full dataset at <https://gnomad.broadinstitute.org>, a browser described in the Data Availability section. Data for all figures is available accordingly. There are no restrictions on the aggregate data released.

Field-specific reporting

Please select the one below that is the best fit for your research. If you are not sure, read the appropriate sections before making your selection.

☒ Life sciences ☐ Behavioural & social sciences ☐ Ecological, evolutionary & environmental sciences

For a reference copy of the document with all sections, see [nature.com/documents/nr-reporting-summary-flat.pdf](https://www.nature.com/documents/nr-reporting-summary-flat.pdf)

Life sciences study design

All studies must disclose on these points even when the disclosure is negative.

Sample size	This study was opportunistic, and involved secondary use of all available genome and exome data. No sample size was predetermined. Nevertheless, the current sample size enables the accurate assessment of constraint against pLoF variation for over 72% of genes in the human genome (see Figure 2).
Data exclusions	Sample QC and variant QC for gnomAD are described extensively in the supplementary methods. Notably, individuals with severe pediatric disease, and known first disease relatives of those with severe pediatric disease were excluded, as previously established and described [Lek et al., 2016].
Replication	We did not attempt to reproduce any findings in a separate dataset, as no other data set of comparable size exists.
Randomization	As this was a population-based study, and not a case-control study, no randomization was performed.
Blinding	As this was a population-based study, and not a case-control study, blinding was not relevant.

Reporting for specific materials, systems and methods

We require information from authors about some types of materials, experimental systems and methods used in many studies. Here, indicate whether each material, system or method listed is relevant to your study. If you are not sure if a list item applies to your research, read the appropriate section before selecting a response.

Materials & experimental systems

n/a	Involved in the study
<input checked="" type="checkbox"/>	<input type="checkbox"/> Antibodies
<input checked="" type="checkbox"/>	<input type="checkbox"/> Eukaryotic cell lines
<input checked="" type="checkbox"/>	<input type="checkbox"/> Palaeontology
<input checked="" type="checkbox"/>	<input type="checkbox"/> Animals and other organisms
<input type="checkbox"/>	<input checked="" type="checkbox"/> Human research participants
<input checked="" type="checkbox"/>	<input type="checkbox"/> Clinical data

Methods

n/a	Involved in the study
<input checked="" type="checkbox"/>	<input type="checkbox"/> ChIP-seq
<input checked="" type="checkbox"/>	<input type="checkbox"/> Flow cytometry
<input checked="" type="checkbox"/>	<input type="checkbox"/> MRI-based neuroimaging

Human research participants

Policy information about [studies involving human research participants](#)

Population characteristics	As an opportunistic collection of data, the participants in this study were not selected based on age, gender, or genotypic information. As described above, individuals with severe pediatric disease, and known first disease relatives of those with severe pediatric disease were excluded. The populations are provided in Supplementary Table 7, and there are 64,754 females and 76,702 males. These data were obtained primarily from case-control studies of adult-onset common diseases, including cardiovascular disease, type 2 diabetes, and psychiatric disorders.
Recruitment	As this was an opportunistic secondary use study, we did not recruit any participants.
Ethics oversight	This study was overseen by the Broad Institute's Office of Research Subject Protection and the Partners Human Research Committee, and was given a determination of Not Human Subjects Research.

Note that full information on the approval of the study protocol must also be provided in the manuscript.